Global simulations of monoterpene-derived peroxy radical fates and the distributions of highly oxygenated organic molecules (HOM) and accretion products

Ruochong Xu[1,2,3], Joel A. Thornton[1]*, Ben H. Lee[1], Yanxu Zhang[2], Lyatt Jaeglé[1], Felipe Lopez-Hilfiker[1,4], Pekka Rantala[5], Tuukka Petäjä[5]

[1] Department of Atmospheric Sciences, University of Washington, Seattle, WA USA 91895
[2] School of Atmospheric Sciences, Nanjing University, Nanjing 210023, China
[3] Now at Department of Earth System Science, Tsinghua University, Beijing 100084, China
[4] Now at Tofwerk AG, Thun Switzerland
[5] Institute for Atmospheric and Earth System Research (INAR) / Physics, University of Helsinki, Helsinki 00014, Finland

*To whom correspondence should be addressed: joelt@uw.edu

Abstract

We evaluate monoterpene-derived peroxy radical (MT-RO_2) unimolecular autoxidation and self and cross reactions with other RO_2 in the GEOS-Chem global chemical transport model. Formation of associated highly oxygenated organic molecule (HOM) and accretion products are tracked in competition with other bimolecular reactions. Autoxidation is the dominant fate up to 6-8 km for first-generation MT-RO_2 which can undergo unimolecular H-shifts. Reaction with NO can be a more common fate for H-shift rate constants < 0.1 s^{-1} or at altitudes higher than 8 km due to the imposed Arrhenius temperature dependence of unimolecular H-shifts. For MT-derived HOM-RO_2, generated by multi-step autoxidation of first-generation MT-RO_2, reaction with other RO_2 is predicted to be the major fate throughout most of the boreal and tropical forested regions, while reaction with NO dominates in temperate and subtropical forests of the Northern Hemisphere. The newly added reactions result in ~4% global average decrease of HO_2 and RO_2 mainly due to faster self-/cross-reactions of MT-RO_2, but the impact upon HO_2/OH/NO_x abundances is only important in the planetary boundary layer (PBL) over portions of tropical forests. Predicted HOM concentrations in MT-rich regions and seasons can exceed total organic aerosol predicted by the standard version of GEOS-Chem model depending on parameters used. Comparisons to observations reveal large uncertainties remain for key reaction parameters and processes, especially the photochemical lifetime and volatility of HOM, and the rates and branching of associated RO_2-accretion products.. Further observations and laboratory studies related to MT-RO_2 derived HOM and gas-phase RO_2accretion product formation kinetics, and especially their atmospheric fate, such as gas-particle partitioning, multi-phase chemistry, and net SOA formation, are needed.

1. Introduction

Monoterpenes are emitted by terrestrial vegetation at a rate of approximately 50 to 100 Tg/yr (Arneth et al., 2008; Guenther et al., 2012; Messina et al., 2016), and are a significant component of volatile consumer products (VCP) (McDonald et al., 2018). Reaction of the

more common monoterpenes, such as α- and β-pinene, Δ-3 carene, and limonene with atmospheric oxidants is rapid, on the timescale of an hour, and produces a suite of semi- (effective saturation concentration, C^* is between 0.3 and 300 $\mu g\ m^{-3}$), low ($3\times10^{-5} < C^* < 0.3$ $\mu g\ m^{-3}$), and extremely low ($C^* < 3\times10^{-5}$ $\mu g\ m^{-3}$) volatility products which contribute to the nucleation and growth of aerosol particles through the formation of secondary organic aerosol (SOA) (Bianchi et al., 2019; Ehn et al., 2014; Hallquist et al., 2009; Kulmala et al., 2014; Palen et al., 1992; Pandis et al., 1992; Zhang et al., 1992). Recent work has shown that even in some isoprene-dominated forested regions, monoterpene oxidation products can be the major component of fine particulate ($PM_{2.5}$) SOA mass (Lee et al., 2020; Xu et al., 2018; Zhang et al., 2018).

Laboratory studies have shown that at least 30 to 50% of the condensable mass produced during oxidation of α-pinene, by both the hydroxyl radical (OH) and ozone, is formed promptly in the first generation of oxidation (Berndt et al., 2016; Ehn et al., 2014; Jokinen et al., 2015; Mentel et al., 2015). This prompt formation of low volatility mass stems from a fraction of the first-generation organic peroxy radicals (RO_2) undergoing repeated unimolecular H-shift reactions followed by O_2 addition, ultimately leading to Highly Oxygenated-organic Molecules (HOM) which are low or even extremely low volatility. The unimolecular H-shifts are the rate-limiting steps to HOM formation, and have been shown for certain RO_2 to exceed 1 s^{-1} at ~296 K (Xu et al., 2019). At such timescales, bimolecular reactions of RO_2 with the hydroperoxy radical (HO_2), other RO_2, and nitric oxide (NO), even if the latter is present at up to 1 ppb, are not competitive, and autoxidation to HOM is expected to be a dominant fate for such RO_2 in the atmosphere. Moreover, the rate constants of corresponding RO_2 cross-reactions, and the branching to accretion products, presumably organic peroxides (ROOR'), have been shown to be substantially larger than previous expectations (Berndt et al., 2018a, 2018b) and important to new particle formation and growth (Bianchi et al., 2019). The ROOR' products can be of low or extremely low volatility as well, even without substantial RO_2 H-shift chemistry, but cross reactions between isoprene-derived RO_2 and MT-HOM RO_2 specifically can be important in limiting ELVOC formation and thus nucleation (Öström, et al., 2017; Roldin et al., 2019; McFiggans et al., 2019).

Relatively few studies to date have evaluated the global implications of such revisions to our understanding of monoterpene (MT) RO_2 fate (Jokinen et al., 2015; Weber et al., 2020; Roldin, et al., 2019; Zhu et al., 2019). Jokinen et al. (2015) showed the impact of MT-HOM formation at specified yields on SOA budgets and CCN. Weber et al (2020) use a condensed reaction mechanism to more explicitly treat the formation of HOM through unimolecular MT-RO_2 autoxidation and cross reactions, but, do not conduct global online simulations. Roldin, et al. 2019 use a similarly explicit mechanism in a 1-D column model to simulate HOM over a boreal forest setting. Zhu, et al. (2019) do not simulate autoxidation and use a less stringent definition of HOM than recommended in Bianchi, et al. (2019). Thus, global-scale simulations with online MT-RO_2 chemistry and comparisons to observations, either using total organic aerosol mass as a constraint or more specific molecular composition measurements of gas and aerosol phase species, remain lacking. Moreover, the

sensitivity of HO_x, O_3, and NO_x abundances and lifetimes to such changes in RO_2 chemistry have yet to be fully explored in global chemical transport models. The unimolecular MT-RO_2 chemistry and faster RO_2 cross reactions have implications for HO_x partitioning, OH recycling, and NO_x lifetime in low-NO_x forested regions. In addition, measurements of highly oxygenated organic nitrates can provide insights into the MT-RO_2 reactivity governing the competitions between autoxidation, RO_2 cross reactions, and RO_2 reactions with nitric oxide (NO).

Herein, we use the GEOS-Chem global chemical transport model to evaluate the impact of MT-RO_2 H-shift and cross-reactions on tropospheric hydrogen oxide radicals (HO_x = OH + HO_2) and total RO_2 abundance, ozone distributions, and assess the potential contribution of MT-HOM and HOM-nitrates to low and extremely low volatility components and by extension the global budget of SOA. We update the GEOS-Chem mechanisms for MT oxidation, using where possible laboratory-derived values of mechanistic parameters, such as MT-RO_2 unimolecular H-shift rate constants, the fraction of MT-RO_2 undergoing H-shifts, and the rate constants for cross-reactions between MT-RO_2 and other RO_2, such as those derived from isoprene oxidation. We compare predicted HOM and HOM-nitrates to atmospheric observations in the gas and particle phases from two locations and conduct sensitivity studies to evaluate the impacts of uncertain kinetic parameters and mechanistic assumptions.

2. Methods

2.1 GEOS-Chem Model

We use the GEOS-Chem chemical transport model (Bey et al., 2001) which is driven by assimilated meteorological fields from the MERRA-2 (Modern-Era Retrospective analysis for Research and Applications, Version 2) (Gelaro et al., 2017). Simulations were conducted with 2°×2.5° LAT × LON horizontal resolution and 47 vertical levels for 28 months from March 2012 to June 2014. This time period provides the best overlap with available observations of monoterpene-derived oxidation products in gas and particle phases made during the SOAS and BAECC field campaigns, described in detail elsewhere (Carlton et al., 2018; Lee et al., 2016, 2018; Lopez-Hilfiker et al., 2016; Petaja et al., 2016), and discussed further below. The first year of the simulation was for spin-up purposes, to allow for accumulation of intermediate chemical reservoir species. For comparison to the observations, we sample the model in time and space corresponding to lowest model grid box containing the location of the observations.

A reference simulation was conducted based on the public version 12.1.0 of GEOS-Chem (http://wiki.geos-chem.org/GEOS-Chem_12#12.1.0). The HO_x-NO_x-VOC-O_3-BrO_x tropospheric chemistry chemical mechanism in the reference simulation is described in Mao et al., (2010, 2013) with recent updates for biogenic VOC chemistry (Fisher et al., 2016; Travis et al., 2016). Emissions of isoprene and monoterpenes are driven by the Model of Emissions of Gases and Aerosols from Nature v2.1 (MEGAN, Guenther et al., 2012). Emissions in GEOS-Chem are based on the Harvard-NASA Emission Component (HEMCO) (Keller et al., 2014). Global anthropogenic emissions of NO_x, SO_2, CO and various aerosol species are from the CEDS (Community Emission Data System) combined with MIX in Asia, NEI in USA, APEI in Canada,

BRAVO in Mexico, EMEP in Europe and DICE in Africa. Open fire emissions are from Global Fire Emissions Database (GFED4). Both gas and aerosol are dry-deposited, with rates calculated online based on the resistance-in-series algorithm (Wesely, 1989; Zhang et al., 2001). Wet deposition is calculated for water-soluble aerosol and gas following (Amos et al., 2012; Liu et al., 2001).

2.2 Updates to the GEOS-Chem MT Oxidation Mechanism

Our goal for the mechanism updates was to preserve as much as possible the current simplified framework for MT chemistry in GEOS-Chem, but to include the essential features of MT-RO_2 unimolecular H-shift and bimolecular RO_2 cross-reactions (see Figure 1). Thus, RO_2 and closed-shell products become quickly lumped into corresponding pools that loosely relate to the dominant functional group character, such as carbonyl, alcohol, nitrate, etc. In this version, we restricted changes to chemistry stemming from OH reaction and ozonolysis only, we do not consider nitrate radical (NO_3) reactions of MT. In what follows, to maintain a higher level of clarity, we mostly discuss the mechanism in general terms. Values of mechanistic parameters can be found in Table S1-S5 and are discussed in more detail in the online supplemental information (SI).

To account for MT-RO_2 H-shift chemistry leading to HOM (i.e. "autoxidation"), we split the first-generation MT-RO_2 formed from the reaction of MT with OH or ozone, into two pools, either MT-aRO_2 or MT-bRO_2. Both types of RO_2 undergo the usual bi-molecular reactions, but MT-aRO_2 do not undergo unimolecular H-shift, while MT-bRO_2 do. The branching between MT-aRO_2 or MT-bRO_2 from MT + OH or MT + O_3 reactions are based on laboratory-derived yields of MT-HOM and MT-nitrates, which typically find that the fraction of MT-RO_2 undergoing autoxidation is <0.5 (Berndt et al., 2016; Kurten et al., 2015; Richters et al., 2016) but can be higher in some studies (Xu et al., 2019). The competitive yields of MT-HOM will be sensitive to the multiplicative product of H-shift rate constants and this fraction of first-generation RO_2 able to undergo autoxidation. As a result, we vary this fraction for both OH and O_3 reactions as part of sensitivity studies.

While MT-aRO_2 do not undergo unimolecular H-shifts, we allow for a small fraction (5%) of MT-aRO_2 reactions involving NO or NO_3 to produce MT-bRO_2 to simulate the corresponding alkoxy radicals undergoing opening of the 4-member ring that is often part of first-generation RO_2 formed from α-pinene ozonolysis and OH reactions (Kurten et al., 2015; Roldin et al., 2019). This fractional fate of the corresponding alkoxy radical is much lower than assumed by Roldin et al. (2019) and thus our estimates in this regard might produce lower HOM concentrations. Iyer et al. (2021) show that prompt C4 ring-opening from α-pinene ozonolysis is possible directly from the Criegee bi-radical, and thus reactions with NO or RO_2 are not necessary for HOM formation. That said, opening of the 4-member ring would lead to second-generation RO_2 structures more amenable to unimolecular H-shift reactions (Iyer et al., 2021; Kurten et al., 2015), and provides a means for enhancing or maintaining HOM formation in the presence of NO as suggested previously (Roldin et al. 2019; Pullinen, et al. 2020), though the balance between alkoxy isomerization and decomposition remains uncertain.

The sequence of autoxidation and base H-shift rate constants used in GEOS-Chem are similar to those described in Pye et al., 2019 for OH oxidation of MT and Jokinen et al. (2015) for MT + O3, which ultimately connect to experimental work in Berndt et al. (2016), Jokinen et al. (2015) and Ehn et al., 2014. The mole fraction of first-generation MT-RO_2 able to undergo unimolecular H-shifts, and thus autoxidation (MT-bRO_2), is 20% from MT + OH and 3% from MT + O_3, in the base simulation (Table S3). The HOM mass yield can be 1.5 to 2 times larger than these molar values. We also note here that GEOS-Chem lumps MT, which can have very different HOM yields, especially from ozonolysis (Ehn et al., 2014). As such, we use the lower reported HOM yields from ozonolysis of α-pinene to reflect the fact that some of the lumped MT will be β-pinene or other MT lacking endo-cyclic double bonds. Our range of sensitivity studies likely capture the associated uncertainty range in these parameters.

A single temperature-dependent rate constant, k_{Hshift}, based upon recent laboratory studies and quantum chemical calculation of associated energy barriers is used to describe these H-shifts. We use an activation energy of 17.7 kcal/mol based on the calculations in Berndt et al., (2016). Two values of k_{Hshift}, near 1.0 s-1 and 0.1 s-1 at 298K, are tested in sensitivity studies. The H-shift reactions of MT-bRO_2 are assumed to be followed by O_2 addition to form a new peroxy radical, MT-cRO_2, which in turn can also continue autoxidation to form a yet more oxidized MT-HOM-RO_2. This sequence of RO_2 autoxidation, occurring in competition with typical bimolecular reactions, simulates a first generation of MT-RO_2, $C_{10}H_{15}O_4$ or $C_{10}H_{17}O_3$, undergoing two H-shift/O_2 addition steps to form RO_2 with compositions of $C_{10}H_{15}O_8$ or $C_{10}H_{17}O_7$, respectively, that are consistent with the current definition of HOM (Bianchi et al., 2019). We do not track autoxidation of non-C_{10} RO_2, and thus our definition of HOM is specific to C_{10} MT products.

These MT-HOM-RO_2 undergo only bimolecular reactions with HO_2, RO_2, NO, and NO_3. Except for RO_2 cross-reactions, discussed further below, rate constants for such reactions are the default values used in GEOS-Chem for other RO_2. The products of these reactions are split into four categories, three of which are HOM. Reaction of MT-HOM-RO_2 with HO_2 is assumed to produce only HOM monomers (aHOM) without a nitrate group. Reaction with NO leads to HOM organic nitrates (HOM-ON), a second class of HOM without a nitrate group (bHOM), and hydroxy carbonyl fragments assumed to be C_5 species. The branching ratio for HOM-ON formation is assumed to be 0.2, determined using typical literature parameterizations based on the carbon number. We explicitly distinguish between non-nitrate HOM that result from reaction of MT-HOM-RO_2 with HO_2 (aHOM) or NO (bHOM) to allow for better accounting of RO_2 fate and the specific impact of NO on HOM. The assumption that the alkoxy radical formation channel of MT-HOM-RO_2 reactions with NO leads to HOM is not well constrained, but it is typically a minor component of the HOM yield on a global average. We neglect further autoxidation reactions of RO_2 and alkoxy radicals, and some of the fragmentation channels of the resulting alkoxy radicals may well produce C9 or C8 products that still meet the HOM definition. Reaction of MT-HOM-RO_2 with the nitrate radical (NO_3) is assumed to produce only an alkoxy radical product (and NO_2), and the alkoxy radical either forms a bHOM (non-nitrate), similar to that from reaction of the RO_2 with NO, or a C_5 hydroxy

carbonyl product to represent fragmentation into non-HOM products. We assume equal branching for these two pathways, which might lead to a slight overestimate of MT-HOM, but reaction with NO_3 is a typically a minor fate for MT-HOM-RO_2.

After addition of RO_2 H-shift chemistry, the next most significant change to monoterpene chemistry we incorporated into GEOS-Chem involves the self- and cross-reactions of RO_2. We specifically evaluated the impact of a higher rate constant and allowed for accretion product formation in competition to the more common alkoxy radical and disproportionation channels which lead to lumped carbonyl (C10-CBYL) and alcohol (C10-OH) products following the typical lumping strategy in GEOS-Chem. Our basis for these changes includes the recent laboratory studies described in Berndt et al., (2018a, 2018b) and Zhao et al., (2018), where cross-reaction rate constants were found to range from 10^{-12} to 10^{-10} cm^3 $molec^{-1}$ s^{-1} and accretion product branching ranged from 4 to >50%. Given that there are only self-reactions for isoprene-derived RO_2 in the current GEOS-Chem without branching to accretion products, taking even the lower range from laboratory studies would represent a major shift in RO_2 fate as we demonstrate in the results section.

Important for regions with intense biogenic VOC emissions and relatively low NO_x (such as regions of the Amazon), we specifically include cross-reactions between monoterpene and isoprene derived RO_2. Our simulations include both low and high estimates of RO_2 self- and cross-reaction rate constants to better demonstrate the range of possible impacts of these reactions, and we also apply different rate constants for highly oxidized RO2 (Table S4). For the rate constants considered, RO_2 cross reactions can become competitive or even dominant fates of RO_2 and thus impact the abundance and recycling of HO_x as well as the formation of low volatility products that would contribute to organic aerosol. For accretion products, we use both a conservative branching (4%) from self- and cross-reactions to produce C20 or C15 compounds, except for HOM-RO_2 self and cross reactions, for which we also examine a larger 100% branching to accretion products as suggested by some laboratory studies (Berndt et al., 2018a, 2018b).

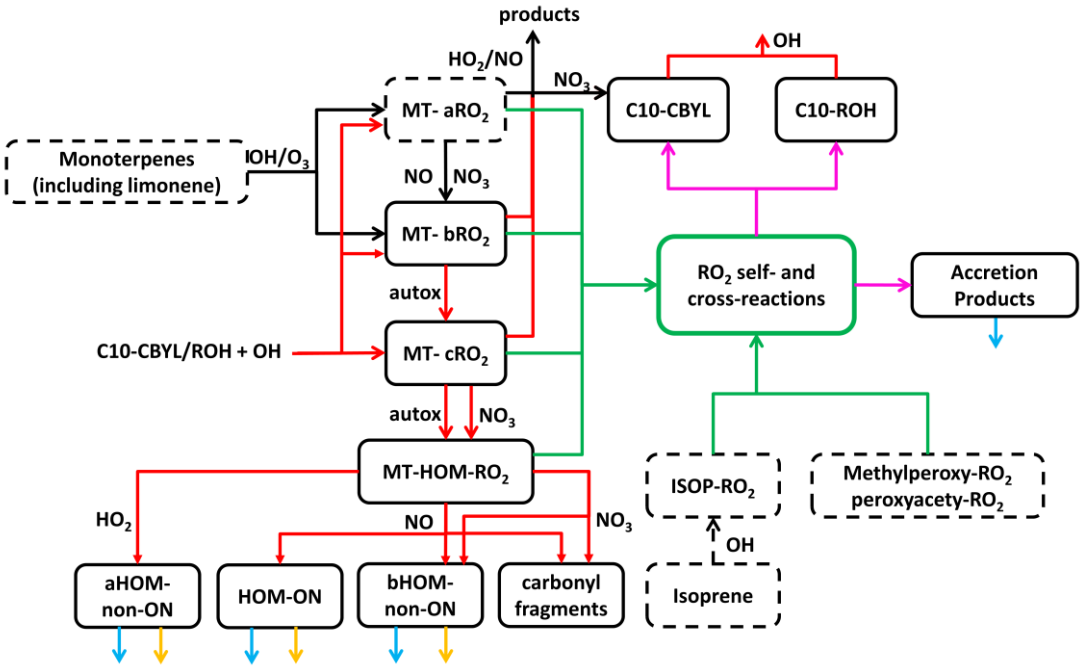

Figure 1. The main reactions and processes included in the updated scheme are shown. Chemical species in solid boxes are newly added while those in dashed boxes already exist in the GEOS-Chem mechanism. Dashed-line black arrows represent originally existing reactions without any modification, and solid black arrows represent those with certain modifications in the scheme. Red, green, and magenta arrows represent newly-added RO_2 formation and loss. Blue and yellow arrows represent dry-/wet-deposition and photolysis, respectively. More details are shown in SI.

We assume the dominant fate of gas-phase MT-HOM as defined here is to partition to existing aerosol particle mass, and then subject to deposition (wet and dry) or by photolysis in the particle phase. While reaction with OH or other radical oxidants is possible, our assumption is that the vast majority of HOM produced in this mechanism will be of low or extremely low volatility and thus be present predominantly in submicron aerosol particles. Our estimates of HOM mass concentrations are therefore possibly upper-limits due to the uncertainty in HOM saturation vapor concentrations. As we do not explicitly consider gas-particle partitioning in this version, we therefore use a single photolysis frequency equal to 1/60 of j_{NO2} to account for photochemical degradation of particle-phase HOM. We do not treat heterogeneous oxidation explicitly, but we assume our photolysis parameterization accounts for this process. The value of the photolysis frequency is based on how well the model reproduces HOM observations in the absence of further photochemical degradation, and also on laboratory chamber experiments showing loss of HOM and associated MTSOA mass over time (Krapf et al., 2016; Pospisilova et al., 2020; Zawadowicz et al., 2020). The photochemical fate of HOM remains one of the most uncertain aspects of the mechanism.

We parameterize HOM wet deposition following aerosol-phase organic nitrate in (Fisher et al., 2016), and dry deposition is calculated online based on the resistance-in-series algorithm (Zhang et al., 2001) assuming HOM behave similarly to SOA (particle dry deposition).

Therefore, the global annually averaged dry deposition velocity of HOM is about 0.06 cm/s on land. The parameters related to aerosol scavenging, rainout and washout efficiency are listed in Table S5 following the parameterization of most secondary organic aerosol species in GEOS-Chem. We note that treating dry deposition of HOM similar to submicron particles is possibly a small underestimate of the actual HOM dry deposition rate because HOM likely condense to particles on timescales shorter than those of dry deposition for vapors in most cases. A typical condensation timescale to aerosol surface area is 15 minutes in the boundary layer, whereas a deposition velocity of 3 cm s^{-1} implies a boundary layer average timescale of several hours. Future updates to the mechanism could consider partitioning of HOM to SOA based on more explicit tracking of composition-volatility relationships, and thus better simulate the net depositional scavenging.

2.3 Simulation Design and Configurations

All simulation configurations are summarized in Table 1. A default simulation without HOM formation nor any other newly-added reactions was run for reference. The base simulation (LowProd_Photo) was run with relatively conservative MT-bRO2 branching, and with HOM photolysis turned on, and another simulation with a larger branching ratio to MT-bRO2 was also run to better determine the HOM formation range (HighProd_Photo). Photolysis of HOM was also turned off to test its impact in LowProd_noPhoto and HighProd_noPhoto cases. Another two simulations configured with slow RO_2 self- and cross-reaction rates (LowProd_Photo_Slow) and slow RO_2 autoxidation rate (LowProd_Photo_kautoSlow) respectively were used to investigate the sensitivity of HOM and accretion products formation to these rates. All simulations were conducted in the same way as described in 2.1. Results were output every month but when comparing with observations, they are output with 1-hour resolution.

Table 1. Simulations and the corresponding configurations. See text for details.

	MT-bRO2 branching	**HOM Photochemical Loss**	**RO_2+RO_2 rates**	**kauto 298 K (s^{-1})**
Default	-	-	-	-
HighProd_noPhoto	high	no	fast	1
HighProd_Photo	high	yes	fast	1
LowProd_noPhoto	low	no	fast	1
LowProd_Photo (base)	low	yes	fast	1
LowProd_Photo_Slow	low	yes	slow	1
LowProd_Photo_kautoSlow	low	yes	fast	0.1

2.4 Observations

Data from three campaigns, the Southern Oxidant and Aerosol Study (SOAS 2013) in the southeastern United States, the Biogenic Aerosols-Effects on Clouds and Climate (BAECC 2014) in Hyytiälä, Finland and the Green Ocean Amazon Experiment (GoAmazon) in Amazon, Brazil were used for comparisons (Carlton et al., 2018; Martin et al., 2016; Petaja et al., 2016). Measurements of organic aerosol mass concentrations from aerosol mass spectrometer

(AMS) instruments (DeCarlo et al., 2006; Jayne et al., 2000) and gas- and particle-phase HOM from High-Resolution Time of Flight Chemical Ionization Mass Spectrometers (HRToF-CIMS) were used when available (Lopez-Hilfiker et al., 2014). For HOM measurements, molecular formulas of compounds containing 10 carbon atoms and greater than or equal to 7 oxygen atoms were selected as HOM for comparisons. Those with one nitrate and without nitrate were compared to simulated HOM-ON and HOM-non-ON, respectively. We also compared predicted HOM to total organic aerosol mass (OA) from aerosol mass spectrometer measurements assuming HOM was present predominantly in submicron aerosol particles. Besides HOM, closely related species in the scheme were also compared when available, including NO, O_3, monoterpenes and isoprene. The details on the measurements were presented in SI including top contributing HOM species identified in data from SENEX and BAECC (Table S7 and S8).

3. Results and discussion

3.1 MT and HOM RO_2 Fates

The largest change to the current mechanism was to the fate of a fraction of MT-derived RO_2, where we incorporated unimolecular autoxidation reactions for a subset of first-generation MT-derived RO_2 (MT-bRO_2 in the above scheme), as well as enhanced reaction rate constants for bimolecular RO_2 self and cross reactions between MT and isoprene RO_2. The fate of RO_2 determines the volatility and reactivity of HOM and thus of the potential for HOM contribution to aerosol formation and growth. In our simplified treatment, we assume HOM-RO_2 only undergo bimolecular reactions. HOM-RO_2 that undergo unimolecular decomposition to a closed-shell product, such as by OH or HO_2 elimination, may result in a non-HOM product. Thus, our flux of MT to HOM-RO_2 may be underestimated, but net HOM production may be more accurate.

The spatial distribution of the annual average reaction fate of MT-bRO_2 in the planetary boundary layer (PBL) is shown in Figure 2 for two simulation cases, LowProd_Photo (panels a-b) and LowProd_Photo_kauto_Slow (panels c-d). The difference between these two simulations is the rate constant for the unimolecular RO_2 H-shift (~$1.0 s^{-1}$ vs. ~$0.1 s^{-1}$ at 298K, respectively). For either case, unimolecular H-shift and subsequent autoxidation is the dominant fate of the first-generation MT-bRO_2 throughout the PBL on average. While likely dependent upon model resolution, when k_auto is ~ 0.1 s^{-1}, the reaction with NO becomes a more common fate for MT-bRO_2, but never more than 50% of the total fate of this HOM-RO_2 precursor, even in NO_x-polluted regions such as the SE U.S., eastern China, and Western Europe. In Figure 3, the annually averaged vertical profiles of MT-bRO_2 fate are shown for two model grid points, one containing Centreville, AL and the other in the Amazon containing the T3 site of the Go-Amazon campaign. The dominance of unimolecular RO_2 H-shift and autoxidation as a fate for MT-bRO_2 persists up to 6 to 8 km, even though its rate is decreasing exponentially with decreasing temperature. In both locations, reaction with NO at high altitudes becomes a major MT-bRO_2 fate, especially over the SE U.S., while over the Amazon reaction with HO_2 and NO above 6 km are of similar importance likely reflecting the combination of the activation energy required for the unimolecular H-shift, decreases in temperature with altitude, and NO in the upper troposphere from lightning and convection.

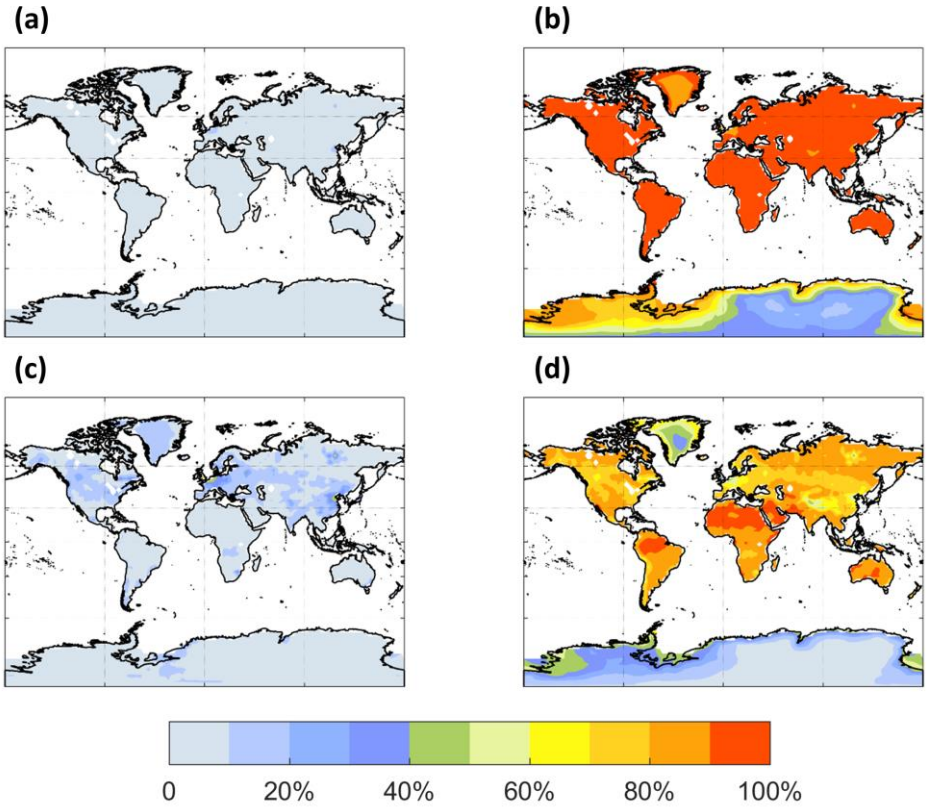

Figure 2. The annually PBL-averaged MT-bRO$_2$ consumption fractions by NO (left panel) and autoxidation (right panel) from experiments LowProd_Photo (a)-(b) and LowProd_Photo_kauto_Slow (c)-(d). Autoxidation rate constant is ~1.0 s^{-1} and ~0.1 s^{-1} at 298K in two experiments, respectively. The fractions by HO_2, NO_3 and RO_2 are shown in Figure S1.

Table 2. Global PBL-average MT-bRO$_2$ fates weighted by gridded MT-bRO$_2$ concentrations on land.

		LowProd_Photo	**LowProd_Photo_kauto_Slow**
MT-bRO$_2$	Autoxidation	93%	77%
	NO	1%	6%
	HO_2	6%	16%
	RO_2	~10^{-4}%	~10^{-3}%
	NO_3	0.4%	1.6%

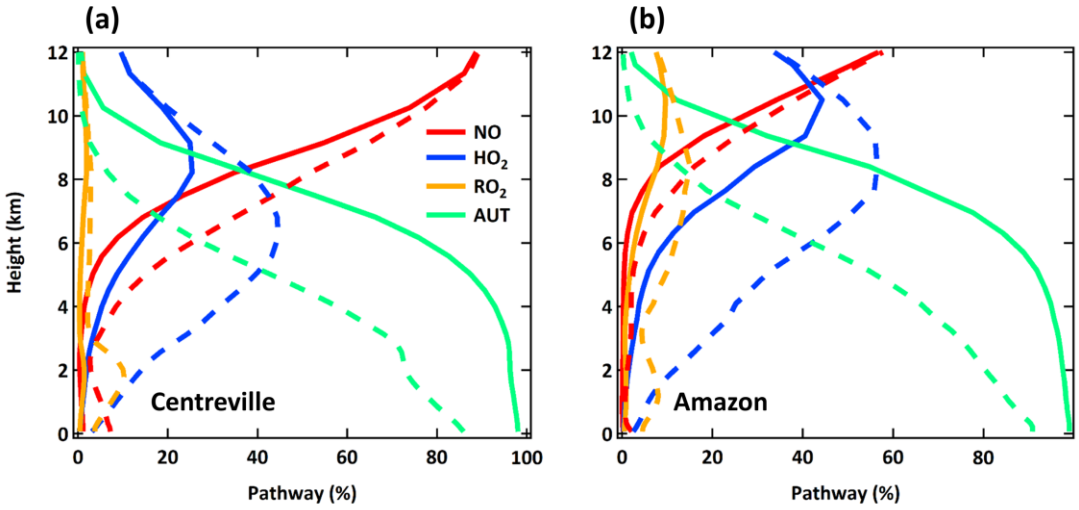

Figure 3. Annual averaged vertical profiles of four dominant reaction pathways of MT-bRO_2 at Centreville, AL USA and over the Amazon near Manaus, from simulations LowProd_Photo (solid lines) and LowProd_Photo_kauto_Slow (dashed lines). Reaction with NO_3 contributes less than 1% and it is thus not shown here.

Figures 4 and 5 are similar to Figures 3 and 4, but for the fates of HOM-RO_2 instead of MT-bRO_2. As HOM-RO_2 in the model do not undergo unimolecular reactions (see above), these fates are more similar to generic RO_2 chemistry in the model with the important exception that the rate constants for self and cross-reactions between HOM-RO_2 and other RO_2 are in general much larger than those typical of other RO_2 in GEOS-Chem. The case where HOM-RO_2 rate constants for RO_2 cross reactions are relatively large (LowProd_Photo, Figure 4 panels a-c), e.g. as in Berndt et al., (2018a), reaction with RO_2 is predicted to be the dominant HOM-RO_2 fate throughout most of the boreal and tropical forest regions as well as portions of the SE US. In temperate and subtropical forests of the N. Hemisphere, reaction with NO is the major fate for HOM-RO_2. The potential importance of reactions with RO_2 being a dominant fate is two-fold. First, the branching of such reactions to accretion products is uncertain (see below), but likely also critical for participation of biogenic VOC in the nucleation of particles (Bianchi et al., 2019; Kulmala et al., 2014). However, the portion of such reactions which do not undergo accretion otherwise can result in less carbon mass moving to lower volatility due to C-C bond scission of alkoxy radical products (Orlando et al., 2003). In the simulation with slower RO_2 cross-reactions (e.g. LowProd_Photo_Slow), rate constants for which are near the lower limit of rate constant collections from several laboratory studies (Berndt et al., 2018a, 2018b; Zhao et al., 2018), RO_2 cross reactions remain important (~40%) across boreal forests, but are no longer dominant as a HOM-RO_2 fate except in the tropical forest regions. Reactions with NO expand in importance in boreal forest regions in this simulation, at times being the dominant fate in regions of the N. American boreal forest. While consistently significant, typically at 30 to 40% of HOM-RO_2 fate, reaction of HOM-RO_2 with HO_2 is only rarely a majority fate in the PBL over forested regions.

The annual average HOM-RO_2 fate changes significantly between the boundary layer and free troposphere as shown in Figure 5 for the same two model locations in Figure 3.

Throughout the low and middle troposphere in both locations, reaction with HO_2 becomes the dominant HOM-RO_2 fate in both locations, followed by RO_2 over the Amazon, and NO over the SE US. Reaction with NO becomes the dominant fate for HOM-RO_2 in the upper troposphere over the SE US, while NO, HO_2 and RO_2 reactions are predicted to be of similar importance over the Amazon.

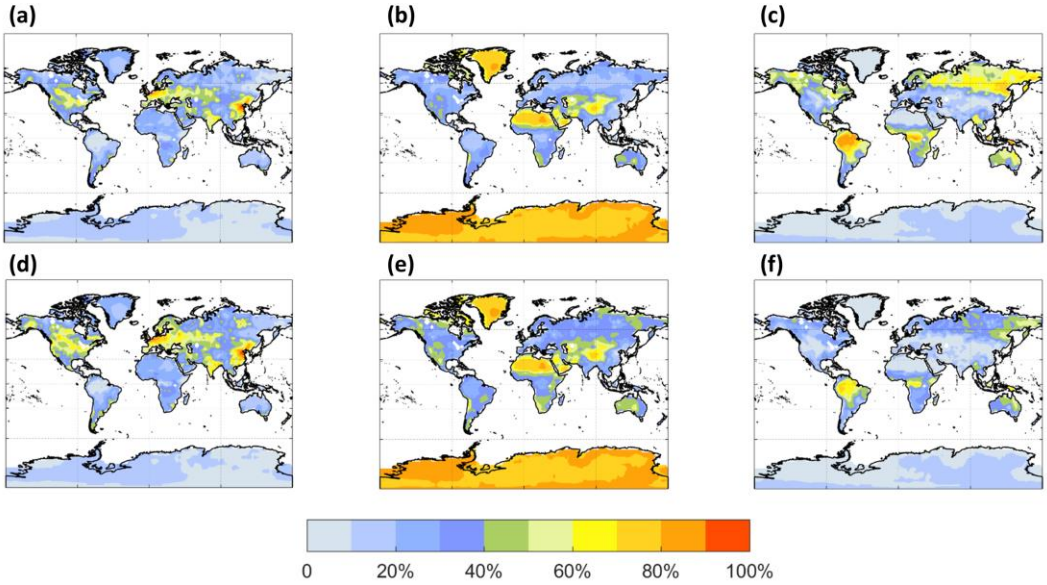

Figure 4. The annually PBL-averaged MT-HOM-RO_2 relative fates including reaction with NO (left panel), HO_2 (middle panel) and RO_2 (right panel) from simulation LowProd_Photo (a)-(c) and LowProd_Photo_Slow (d)-(f). Reaction with NO_3 contributes <1% and it is thus not shown here.

Table 3. Global PBL-average MT-HOM-RO_2 fates weighted by gridded MT-HOM-RO_2 concentrations on land.

		LowProd_Photo	**LowProd_Photo_Slow**
MT-HOM-RO_2	NO	16.44%	20.71%
	HO_2	22.00%	33.12%
	RO_2	61.54%	46.11%
	NO_3	0.02%	0.06%

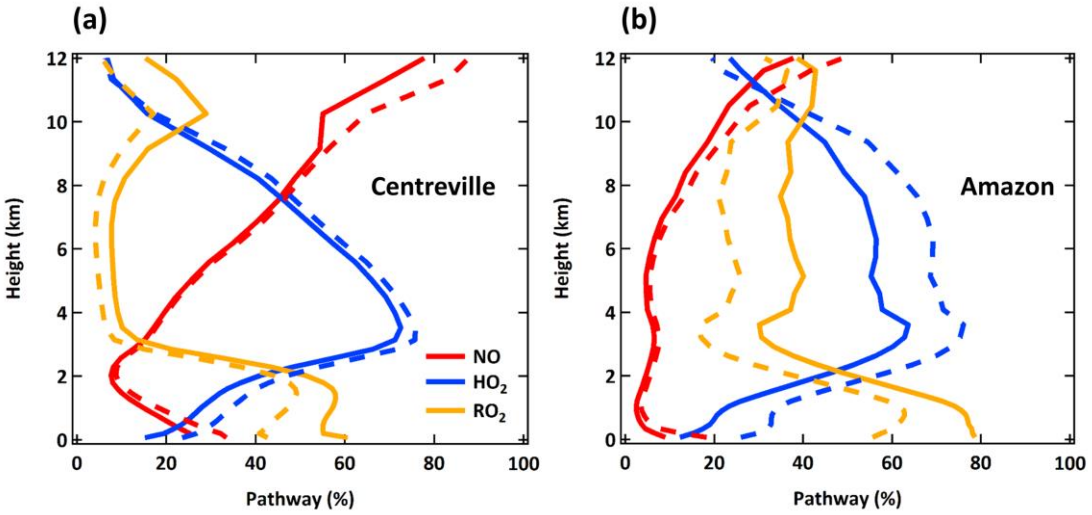

Figure 5. Annual averaged vertical profiles of three dominant reaction pathways of MT-HOM-RO_2 at Centreville, AL and Amazon near Manaus, from simulation LowProd_Photo (solid lines) and LowProd_Photo_Slow (dashed lines). Reaction with NO_3 contributes < 1% and it is thus not shown here.

3.2 Impact on HO_x, NO_x, and O_3

By altering the fates of MT-derived RO_2 chemistry and the interactions thereof with isoprene-derived RO_2, we expect that the cycling and lifetime of HO_x are affected. Changes in HO_x abundance and distribution will alter NO_x cycling and fate, which will potentially impact tropospheric O_3. MT are not typically major components of OH reactivity, even in biogenically influenced regions so these impacts are not expected to be large. As shown in Figure 6, there are substantial decreases in the sum of HO_2 and RO_2 concentrations in certain regions averaged over the planetary boundary layer (PBL), the height of which is taken from the MERRA-2 reanalysis data (Gelaro et al., 2017). HO_2 and RO_2 concentrations together decrease by as much as ~20% over boreal forests and up to 80% over tropical forests. The global average decrease in the sum of HO_2 and RO_2 in this simulation compared to the default is 4%. The updated description of RO_2 self and cross reactions is the dominant driver of the shorter RO_2 lifetime and thus of the calculated decreases. Given that most of these decreases in RO_2 occur in locations with low NO, the impact upon HO_2 and OH (Figure 6b) are small globally, but not negligible in the PBL over the Amazon, reaching a ~15% decrease in OH. The lower OH predicted over the Amazon leads to longer NO_x lifetimes there and thus a highly localized increase in NO_x abundance. Otherwise, the effects on NO_x and O_3 are negligible globally.

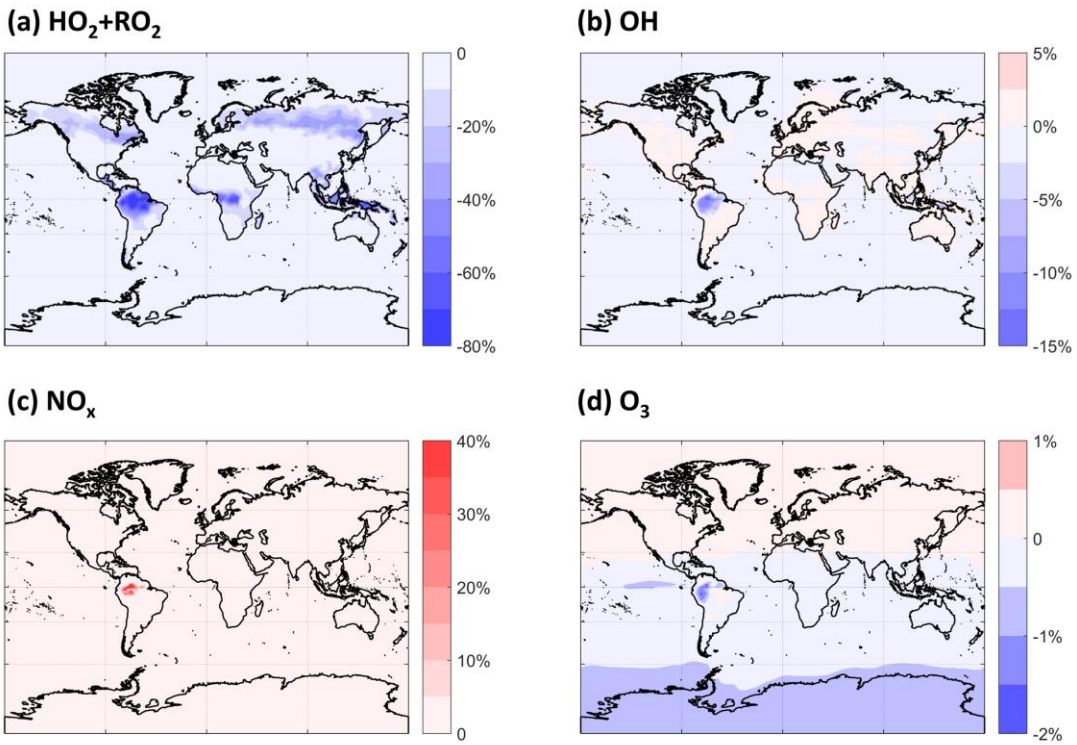

Figure 6. The annual PBL-averaged relative differences of (a) HO_2+RO_2, (b) OH, (c) NO_x and (d) O_3 between simulations LowProd_Photo and Default.

3.3 HOM and associated accretion product distribution and concentrations

Table 4. Global annual budgets of MT-HOM and MT-RO_2 accretion products from Mar. 2013 to Feb. 2014 (unit: kt C).

	Chemistry	Wet deposition	Dry deposition
HOM-non-ON	321	-277	-45
HOM-ON	26	-20	-6
Total accretion products	2107	-1907	-204

Global annual budgets for the chemistry (Production + Loss), and wet and dry deposition of HOM-non-ON, HOM-ON and MT-derived accretion products are summarized in Table 4 from the LowProd_Photo_kauto_slow simulations. For even the slowest kauto used, the non-nitrate pathway for HOM is more than factor of 10 that of HOM organic nitrates. Interestingly, even for a small branching to accretion products, MT-RO_2 derived accretion products are a substantially larger fate than HOM, suggesting either that the rates and branching are too high or that the chemical loss pathways of associated products are not well represented.

The PBL average mass concentrations (μg m^{-3}) of HOM predicted by the model are shown in

Figure 7 (a-d) for the LowProd_noPhoto, which produces middle-to-upper range estimates of HOM concentrations out of the other scenarios tested. Maps from other sensitivity simulations are included in the SI (Figure S2-S6). In this scenario, monoterpene-derived HOM are predicted to average near 1 μg m^{-3} in the PBL over tropical forests with little seasonality, while in the temperate and boreal forests of N. America, Europe, and east Asia, HOM reach 0.5 to 1 μg m^{-3} during summer months. In the LowProd_Photo scenarios, HOM concentrations average an order of magnitude lower than shown in Figure 7, though the spatial and seasonal patterns are similar. Given that HOM with 10 carbons and 7 or more oxygens will be low or extremely low volatility, the majority of HOM produced from monoterpene oxidation will likely contribute to SOA and thus to total OA. A background organic aerosol mass concentration in rural or remote forested regions of order 1 μg m^{-3} outside of biomass burning periods is not atypical (Jimenez et al., 2009).

For comparison, we also show seasonal PBL distributions of HOM-RO_2 self or cross reaction accretion products, assuming the C_{20}-HOM are formed at unit yield. This assumption provides an upper-limit, but one which is supported by some laboratory studies (Berndt et al., 2018a and b). Throughout the tropical forests and boreal regions during summer, HOM-RO_2 accretion products in this simulation reach 3 or 1 μg m^{-3}, respectively. As total OA in some boreal and tropical forest measurements can be on this order (Jimenez et al., 2009; Lee et al., 2018; de Sa et al., 2018) outside of biomass burning periods, we conclude C_{20}-HOM undergo particle phase decomposition and/or the HOM-RO_2 self and cross reactions do not produce accretion products at unit yield or the model underestimates NO throughout boreal and tropical forest regions which would suppress both HOM and more so HOM accretion product concentrations. As shown in the SI (Figure S7), assuming an accretion product branching of 4% for all MT-RO_2 self or cross reactions as in Zhao, et al. (2019), including HOM-RO_2, leads to significantly lower, but not unimportant, concentrations of accretion products. The total C_{15} + C_{20} accretion product concentrations in the PBL of tropical and boreal forest regions are typically less than 1 or 0.25 ug m^{-3}, respectively, in this simulation.

Accretion products from HOM-RO_2 reactions with other HOM-RO_2 are likely an important route to new particle formation especially in the relatively warm planetary boundary layer. Thus, to predict new particle formation in regions such as the remote temperate or boreal forests, such accretion products will need to be incorporated. As noted above, the self and cross reaction rates and accretion product branching in both cases are far larger than those commonly used in GEOS-Chem. Nucleation and growth of particles by MT-HOM and associated accretion products is beyond the scope here, but in both treatments of accretion product formation, C_{20} HOM accretion products reach concentrations which are likely relevant for participation in new particle formation (e.g. 10^7-10^8 molec cm^{-3}) to the extent it occurs in the PBL over forested regions (Bianchi et al., 2019). A remaining question is to what extent MT-RO_2 derived accretion products more generally form and contribute to OA mass.

Our results suggest that further refinement of HOM formation and loss kinetics is needed since the range of our simulations suggest HOM either make relatively small contributions to

regional OA or constitute the majority of OA outside of biomass burning periods over tropical forests year-round, and during summer months for temperate and boreal forests. Figure 8 illustrates that for two of the sensitivity simulations which bound possible HOM formation and loss kinetics, MT-HOM concentrations alone are either 5 to 10% of total OA predicted by the standard GEOS-Chem model or are more than a factor of 1.5 higher than the predicted total OA. Incorporating predicted MT-RO_2 derived C_{15} and C_{20} accretion products as an OA source only increases the potential contribution of MT to total OA. If the MT-RO_2 accretion product branching is on average 4%, accretion products can double the contribution of MT to OA when HOM are simulated in the LowProd_Photo case (see Figure S7). If the accretion branching ratio is closer to unity, as expected for HOM-RO_2, the contribution of HOM monomers and MT-HOM accretion products to OA is even larger, reaching or exceeding a mean ratio of 3 in tropical forests compared to GEOS-Chem predicted OA. Thus, revising MT chemistry to incorporate gas-phase sources of low and extremely low volatility pathways will likely increase, perhaps substantially, the total OA predicted by the GEOS-Chem model over forested regions.

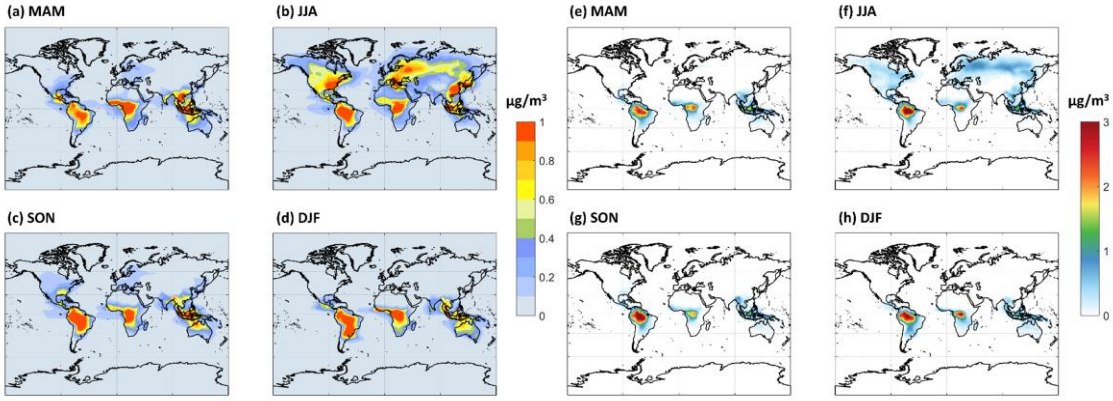

Figure 7. The seasonal PBL-averaged total HOM mass concentrations of (a) MAM, (b) JJA (c) SON and (d) DJF from experiment LowProd_noPhoto. Seasonal PBL-averaged total C_{20} HOM accretion products are shown in panels e-h, assuming HOM-RO_2 self and cross reactions produce accretion products at unit yield.

There are limited observations of HOM that can be used to investigate the validity of the different scenarios simulated here. First, the majority of HOM will condense to form SOA, where they may further react to form products that might not be traceable to HOM formed in the gas-phase (Krapf et al., 2016; Lee et al., 2020; Pospisilova et al., 2020; Zawadowicz et al., 2020). Second, most HOM have been observed only in the gas-phase (Bianchi et al., 2016; Ehn et al., 2014; Massoli et al., 2018), which represents only a local steady-state between the formation and condensation sink over small spatial scales compared to the current model resolution. The FIGAERO HRToF-CIMS instrument measures some HOM in both the gas and particle phases, while the aerosol mass spectrometer (AMS) provides an upper limit constraint on the total organic aerosol. In Figure 8, we show observations from the FIGAERO HRTOF-CIMS at a rural temperate and rural boreal forest, in Centreville, AL in the Southeast U.S. and SMEAR II station in Hyytiälä, Finland, respectively, using only C_{10} compounds. In

addition, we show AMS observations of total OA from these sites as well as from the T3 site of the Go-Amazon campaign outside of Manaus, Brazil. The Centreville, AL observations were obtained in June-July 2013, the SMEAR II observations were from April –June 2014, and the Go-Amazon observations were from February-March 2014. More information can be found in SI and related papers (Carlton et al., 2018; Martin et al., 2016; Petaja et al., 2016). The FIGAERO HRToF-CIMS observations include both speciated HOM organic nitrates and non-nitrates.

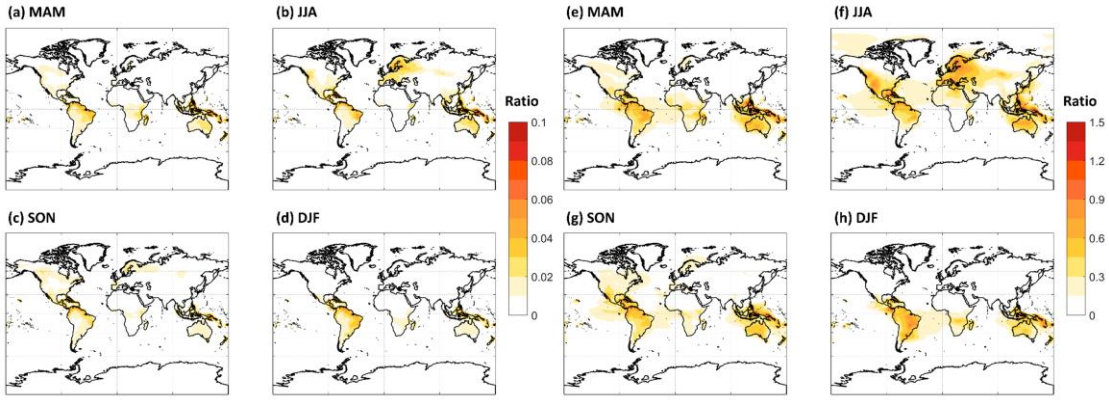

Figure 8. The seasonal PBL-averaged total C_{10}-HOM mass concentrations from the LowProd_Photo (a-d) or the HighProd_noPhoto (e-h) simulations plotted relative to the total OA mass concentration predicted by GEOS-Chem for the same periods and locations. Note the color scale for panels a-d (0 to 0.1) is about a factor of 10 lower than that for panels e-h (0 to 1.5).

We compare these observations to two simulations, HighProd_Photo and LowProd_Photo, where each includes photochemical losses of HOM based on recent experimental work (Zawadowicz et al., 2020), but different yields of MT-bRO_2 that can undergo unimolecular H-shifts as discussed above. The comparison is challenged for a number of reasons. First, monoterpene emissions are uncertain in a global sense but will also vary significantly at scales below the resolution of the model. Second, gas-phase HOM will be sensitive to the local oxidant conditions, which will also depend on model predicted NO concentrations and BVOC, while particulate HOM potentially represent the integral of multiple days of formation, loss, and transport. Moreover, HOM in the particle phase may react into non-HOM, be lost on instrument surfaces, or thermally decompose during the analysis, such that observations of total HOM are possibly underestimated by the FIGAERO HRToF-CIMS instrument. To facilitate the comparison, we use the diurnal cycle in observations averaged over 4 to 6 weeks of observations to minimize the impact of meteorological variability. Addressing errors in the MEGAN emissions inventory is beyond the scope of this paper, therefore, we scale the predicted HOM concentrations in the lowest model level by the ratio of observed to predicted monoterpene concentrations in order to account for potential biases in the regional monoterpene emissions in the model (Figure S8). For SOAS and GoAmazon, we use the hourly average measured monoterpene data to compare with the hourly GEOS-Chem predictions, while for the BAECC campaign at SMEAR II station, we use the campaign average of measured monoterpene concentrations. We separate HOM organic nitrates (ON) from HOM non-nitrates (non-ON) where possible but compare to the total measured gas + particle

in each category.

As shown in Figure 9, there is general order-of-magnitude agreement between the observed HOM and those predicted by one of the model simulations when adjusted by the predicted and observed monoterpene concentrations as described above. The HighProd_Photo simulation is better able to simulate the HOM-ON, but overestimates the non-ON HOM measured in the boreal forest location. In contrast, in the Centreville location, the HighProd_Photo simulation underestimates the measured HOM-ON but overestimates the measured non-ON HOM. The general overestimation of observed non-ON HOM could be due to the non-ON HOM having reacted in the particle phase into components that are not detectable as HOM due to analytical limitations of the instrument used, which relies on thermal desorption and thus can be subject to thermal decomposition of low volatility components [Lopez-Hilfiker et al., 2014]. We note that the HighProd_Photo simulation does not overestimate the observed fine mode OA mass concentrations in any of the three locations, such that there is potential for a higher fraction of MT oxidation to result in HOM and higher contributions of MT-HOM to OA than shown in Figure 9. The reason for a low contribution of MT-HOM to OA predicted for the Amazon region remains unknown, but possibly related to errors in the modeled MT emission inventory, limitations of comparing a relatively coarse model resolution to a single location measurement, and/or the influences from isoprene, biomass burning, and other pathways are perhaps more important in this location.

The general shape of the HOM diurnal cycle and HOM relative to OA (Figure 9) are typically well captured for each location, except for the late evening and early morning periods possibly due to issues simulating the nocturnal layer relative to the emission height of monoterpenes. In the Amazon location, there is a clear late afternoon peak in the measured OA that is not present in the predicted monoterpene derived HOM concentrations. These comparisons suggest that based on the current set of observations we cannot conclude which set of HOM formation and loss kinetics is most appropriate for describing ambient HOM. We can conclude that total HOM abundances, including both ON and non-ON HOM, are potentially higher than those shown in Figure 9, similar to those predicted by the HighProd_Photo case or the LowProd_noPhoto case, with PBL average mass concentrations in monoterpene rich regions and seasons of order 0.5 to 1 $\mu g\ m^{-3}$, see, e.g., Figures S9 and S10. Uncertainties in first-generation RO_2 branching parameters, isomerization rate constants, and HOM chemical fate remain large, with limited observational constraints on total HOM concentrations (gas + particle).

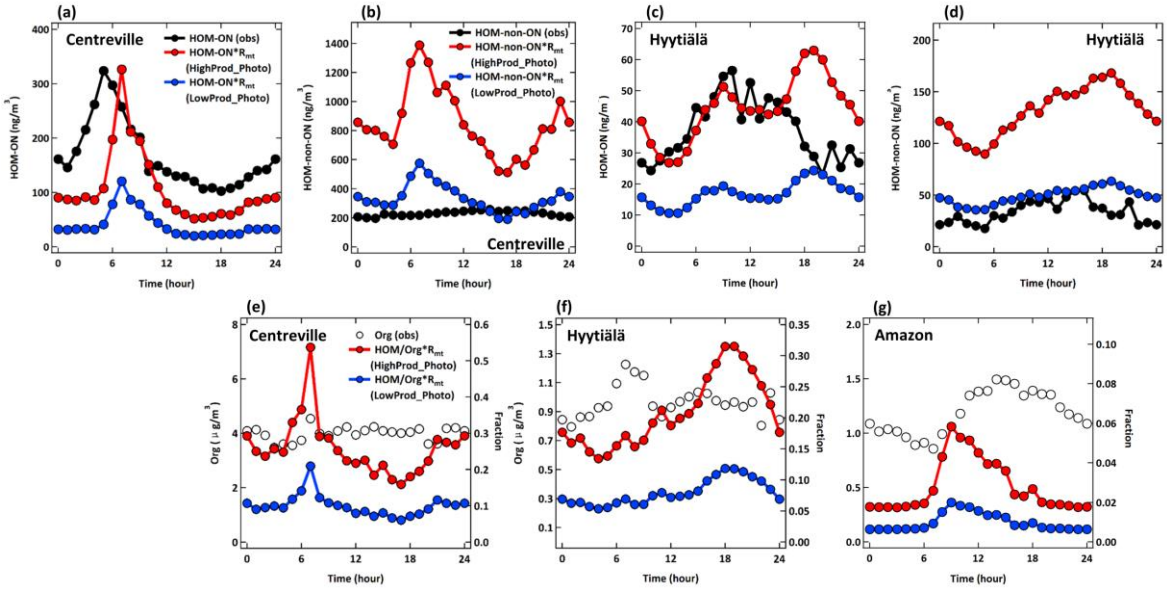

Figure 9. Diurnal changes of observed (black line) and simulated (HighProd_Photo: red line; LowProd_Photo: blue line) (a) HOM-ON and (b) HOM-non-ON mass concentrations at Centreville site. (c)-(d) The same as (a)-(b) but at Hyytiälä site. (e)-(f) Diurnal changes of observed organic aerosol mass concentrations (black hollow circle markers) and the fractions that simulated total HOM account for of observed organic aerosols (HighProd_Photo: red; LowProd_Photo: blue) at Centreville, Hyytiälä and Amazon sites, respectively.

3.4 Vertical profiles of HOM

Figure 10 summarizes the vertical distribution of HOM predicted by the LowProd_Photo simulation for two locations, one over the SE US SOAS site and one over the Amazon region using the same grid which contains the GoAmazon T3 site (Martin et al., 2016). Evident is the expected predominance of monoterpene present within the PBL in all seasons and locations related to the surface vegetation source. Also evident is the different vertical profiles of HOM-ON compared to non-ON HOM, with slower decays with altitude of non-ON HOM up to 2 to 3 km above the surface during JJA in both the SEUS and Amazon regions, likely due to changes in the HOM-RO2 fate with altitude (see 3.1). Over the Amazon during JJA and SON, both non-ON HOM and HOM-ON concentrations are predicted to be relatively enhanced between 1 to 5 km compared to the lowest altitude concentrations. The relative enhancement in this altitude region during JJA and SON compared to DJF and MAM likely reflects overall drier conditions but also significant vertical transport of HOM precursors during these seasons, e.g. through shallow convection. The relative enhancements specifically between 1 to 4 km compared to altitudes higher than 5km could also reflect the temperature dependence of the unimolecular H-shift rate constant describing monoterpene derived RO_2 autoxidation and changing biomolecular reaction rates with altitude. This relative enhancement is not as obvious in the vertical profiles over the SEUS, which appear as smoother monotonic decays with altitude, and that are higher in abundance during summer months.

HOM-RO_2 accretion products illustrate similar vertical profiles as the HOM monomers (see SI

Figures S12 and S13). If we use the rate constants reported by Berndt et al., (2018a, 2018b) together with branching ratio of unity for HOM-RO_2 derived accretion products, the seasonal mean abundance of predicted total of C_{15} and C_{20} HOM accretion products reaches 1 to 5 μg m^{-3} in the PBL over the SE US and tropical forested regions respectively (see SI), and decay to $1x10^{-3}$ and $3x10^{-2}$ μg m^{-3} ($1x10^6$ and $4x10^7$ molec cm^{-3}), respectively, in the upper troposphere over these regions. Assuming instead a HOM-RO_2 accretion product yield of 4%, the predicted total of C_{15} and C_{20} HOM accretion products are between 0.2 and 1 μg m^{-3} over the SE US and tropical forests, respectively, decaying to $2x10^{-4}$ and $7x10^{-3}$ μg m^{-3} ($3x10^5$ and $1x10^7$ molec cm^{-3}) in the upper troposphere. At such *average* concentrations in the upper troposphere over these regions, we conclude either type of HOM accretion product will likely contribute significantly to new particle formation and growth, but uncertainty in the accretion product branching of HOM-RO_2 reactions would lead to a factor of 4 or more in the estimated contribution.

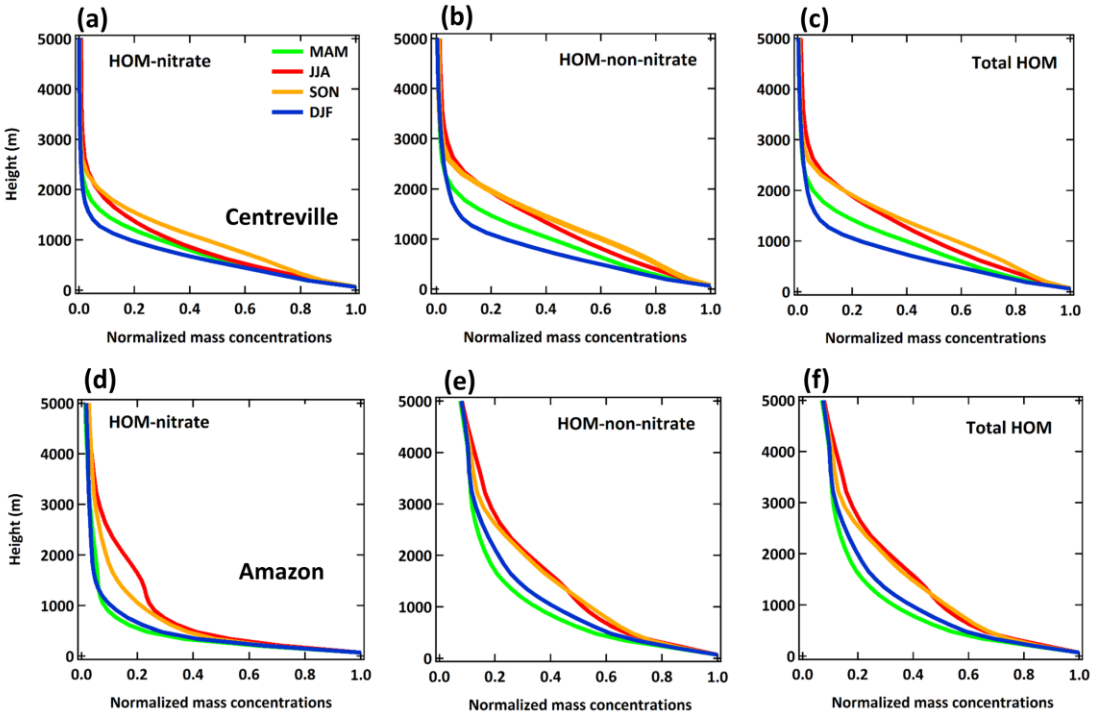

Figure 10. The seasonal averaged vertical profiles of HOM-ON (left panel), HOM-non-ON (middle panel) and total HOM (right panel) at Centreville (top panel) and Amazon (bottom panel). All the results are from experiment LowProd_Photo. Values are normalized to the lowest-level values of each season. The profiles with absolute concentrations are shown in Figure S9.

4. Conclusion

We implemented a new mechanism to describe MT-derived RO_2 chemistry in the GEOS-Chem global chemical transport model. The mechanism is relatively simple, adding 10 species and 37 reactions to the standard mechanism, without substantial addition of computation time. We focused on updating the representation of unimolecular H-shift reactions to form HOM-RO_2 and their fate, as well as the self- and cross-reactions of

MT-derived RO_2 and isoprene derived RO_2. Several sensitivity studies were conducted to evaluate the impact of various mechanism parameters and associated uncertainties, and where possible we compared to observations. The results from these sensitivity studies show that for a model resolution of 2^o x 2.5^o, uncertainty in the average H-shift rate constant is less important for predicted HOM concentrations than the fraction of MT reactions with OH or O_3 to form RO_2 which can undergo H-shift and autoxidation and the photochemical lifetime of HOM. While a comprehensive comparison of HOM predictions to OA remains, in three locations, the model predictions of HOM did not exceed total measured OA mass concentrations, which is currently the strongest constraint on HOM. However, using HOM-ON measurements as a guide suggests that if the fraction of MT-RO_2 that undergo relatively rapid H-shift (k_{auto} > 0.1 s^{-1}) is greater than 0.25, then significant photochemical losses of HOM mass from particles that is faster than wet or dry deposition of particulate organics is required. Indeed, the current estimates of MT-derived HOM monomer and HOM accretion product formation rates from laboratory studies lead to mass concentrations of the same order as or event OA mass concentrations predicted by the model. However, uncertainties in emission inventories of BVOC and small absolute errors in NO or NO_3 concentration fields in global scale models contribute additional uncertainty into the most appropriate set of parameters to use.

The majority of HOM production occurs in the continental boundary layer where MT emissions are significant, including boreal, temperate and tropical regions. H-shift and autoxidation is the major fate for the subset of MT-RO_2 with that capability, outcompeting reactions with NO, HO_2 and RO_2 up to 6 km altitude in relatively unpolluted regions. Autoxidation of first-generation MT-RO_2 is significantly slower in the upper troposphere and likely uncompetitive with reactions with NO and HO_2. As such, HOM formation in the outflow of deep convection is unlikely, though HOM formation from MT detraining from shallow convection below 6 km is feasible.

Implementing faster self and cross-reactions between RO_2 in GEOS-Chem as found by Zhao et al. (2019) and Berndt et al. (2018a) lead to significantly lower HO_2 and RO_2 concentrations in boreal and tropical forested regions (by 20% or more compared to the standard mechanism), but globally average changes in OH, NO_x, and O_3 are negligible. These reactions also alter the fate of MT-RO_2, especially MT-derived HOM-RO_2, for which reaction with MT-derived and other RO_2 (typically isoprene-derived) is the dominant fate throughout the boundary layer neglecting unimolecular HOM-RO_2 reactions. While perhaps unexpected compared to previous RO_2 fate assessments using slower RO_2 self and cross reaction rate constants, such a situation can be supported in part by the molecular composition measurements of MT-HOM which show significant contributions of HOM with H numbers less than 16 and odd-numbers of O, e.g., $C_{10}H_{14}O_9$. This evidence alone is not sufficient, as HOM-RO_2 reactions with NO could also produce similar results. Future field campaigns that constrain the relevant NO_x and oxidant fields together with HOM in low-NO_x regions could provide important constraints in this regard.

The branching to accretion products of RO_2 self and cross reactions is a key parameter with significantly different ranges produced by laboratory studies. The concentrations of C_{15} and C_{20}

accretion products predicted using self and cross-reaction rate constants of ~10^{-11}-10^{-10} cm^3 $molec^{-1}$ s^{-1} with a conservative branching (4%) from Zhao et al (2018), are typically small compared to average OA mass concentrations, except in the tropical forested regions, where these accretion products alone are likely similar to background OA concentrations outside of biomass burning events. Using a larger branching to accretion products as supported by studies by Berndt et al (2018) leads to such accretion products likely dominating low volatility products that could contribute to OA, with predicted mass concentrations well exceeding OA mass concentrations in remote tropical regions. Thus, further refinement in the rate constants and branching to gas-phase accretion products and their photochemical fates are needed, especially since these products from HOM-RO_2 cross reactions are likely essential in the contributions of MT to new particle formation (Bianchi et al., 2019; McFiggans et al., 2019) especially over tropical forested regions (Andreae et al., 2018; Wang et al., 2016; Zhao et al., 2020).

Acknowledgements

JAT was supported by a grant from the National Science Foundation (CHE-1807204) and the U.S. Department of Energy Atmospheric Science Research program (DE-SC0021097). RX thanks Nanjing University for an undergraduate research fellowship.

References Cited

Amos, H. M., Jacob, D. J., Holmes, C. D., Fisher, J. A., Wang, Q., Yantosca, R. M., Corbitt, E. S., Galarneau, E., Rutter, A. P., Gustin, M. S., Steffen, A., Schauer, J. J., Graydon, J. A., St Louis, V. L., Talbot, R. W., Edgerton, E. S., Zhang, Y. and Sunderland, E. M.: Gas-particle partitioning of atmospheric Hg(II) and its effect on global mercury deposition, Atmos. Chem. Phys., 12(1), 591–603, doi:10.5194/acp-12-591-2012, 2012.

Andreae, M. O., Afchine, A., Albrecht, R., Holanda, B. A., Artaxo, P., Barbosa, H. M. J., Borrmann, S., Cecchini, M. A., Costa, A., Dollner, M., Fuetterer, D., Jaervinen, E., Jurkat, T., Klimach, T., Konemann, T., Knote, C., Kraemer, M., Krisna, T., Machado, L. A. T., Mertes, S., Minikin, A., Poehlker, C., Poehlker, M. L., Poeschl, U., Rosenfeld, D., Sauer, D., Schlager, H., Schnaiter, M., Schneider, J., Schulz, C., Spanu, A., Sperling, V. B., Voigt, C., Walser, A., Wang, J., Weinzierl, B., Wendisch, M. and Ziereis, H.: Aerosol characteristics and particle production in the upper troposphere over the Amazon Basin, Atmos. Chem. Phys., 18(2), 921–961, doi:10.5194/acp-18-921-2018, 2018.

Arneth, A., Monson, R. K., Schurgers, G., Niinemets, Ü. and Palmer, P. I.: Why are estimates of global terrestrial isoprene emissions so similar (and why is this not so for monoterpenes)?, Atmos. Chem. Phys., 8(16), 4605–4620, doi:10.5194/acp-8-4605-2008, 2008.

Berndt, T., Richters, S., Jokinen, T., Hyttinen, N., Kurtén, T., Otkjær, R. V., Kjaergaard, H. G., Stratmann, F., Herrmann, H., Sipilä, M., Kulmala, M. and Ehn, M.: Hydroxyl radical-induced formation of highly oxidized organic compounds, Nat. Commun., 7(May), 13677, doi:10.1038/ncomms13677, 2016.

Berndt, T., Mentler, B., Scholz, W., Fischer, L., Herrmann, H., Kulmala, M. and Hansel, A.: Accretion Product Formation from Ozonolysis and OH Radical Reaction of α-Pinene: Mechanistic Insight and the Influence of Isoprene and Ethylene, Environ. Sci. Technol., doi:10.1021/acs.est.8b02210, 2018a.

Berndt, T., Scholz, W., Mentler, B., Fischer, L., Herrmann, H., Kulmala, M. and Hansel, A.:

Accretion Product Formation from Self- and Cross-Reactions of RO2 Radicals in the Atmosphere, Angew. Chemie Int. Ed., 57(14), 3820–3824, doi:https://doi.org/10.1002/anie.201710989, 2018b.

Bey, I., Jacob, D. J., Yantosca, R. M., Logan, J. A., Field, B. D., Fiore, A. M., Li, Q.-B., Liu, H.-Y., Mickley, L. J. and Schultz, M. G.: Global Modeling of Tropospheric Chemistry with Assimilated Meteorology: Model Description and Evaluation, J. Geophys. Res., 106, 73–95, doi:10.1029/2001JD000807, 2001.

Bianchi, F., Trostl, J., Junninen, H., Frege, C., Henne, S., Hoyle, C. R., Molteni, U., Herrmann, E., Adamov, A., Bukowiecki, N., Chen, X., Duplissy, J., Gysel, M., Hutterli, M., Kangasluoma, J., Kontkanen, J., Kuerten, A., Manninen, H. E., Muench, S., Perakyla, O., Petaja, T., Rondo, L., Williamson, C., Weingartner, E., Curtius, J., Worsnop, D. R., Kulmala, M., Dommen, J. and Baltensperger, U.: New particle formation in the free troposphere: A question of chemistry and timing, Science (80-.)., 352(6289), 1109–1112, doi:10.1126/science.aad5456, 2016.

Bianchi, F., Kurten, T., Riva, M., Mohr, C., Rissanen, M. P., Roldin, P., Berndt, T., Crounse, J. D., Wennberg, P. O., Mentel, T. F., Wildt, J., Junninen, H., Jokinen, T., Kulmala, M., Worsnop, D. R., Thornton, J. A., Donahue, N., Kjaergaard, H. G. and Ehn, M.: Highly Oxygenated Organic Molecules (HOM) from Gas-Phase Autoxidation Involving Peroxy Radicals: A Key Contributor to Atmospheric Aerosol, Chem. Rev., 119(6), 3472–3509, doi:10.1021/acs.chemrev.8b00395, 2019.

Carlton, A. G., de Gouw, J., Jimenez, J. L., Ambrose, J. L., Attwood, A. R., Brown, S., Baker, K. R., Brock, C., Cohen, R. C., Edgerton, S., Farkas, C. M., Farmer, D., Goldstein, A. H., Gratz, L., Guenther, A., Hunt, S., Jaeglé, L., Jaffe, D. A., Mak, J., McClure, C., Nenes, A., Nguyen, T. K., Pierce, J. R., de Sa, S., Selin, N. E., Shah, V., Shaw, S., Shepson, P. B., Song, S., Stutz, J., Surratt, J. D., Turpin, B. J., Warneke, C., Washenfelder, R. A., Wennberg, P. O. and Zhou, X.: Synthesis of the Southeast Atmosphere Studies: Investigating Fundamental Atmospheric Chemistry Questions, Bull. Am. Meteorol. Soc., 99(3), 547–567, doi:10.1175/BAMS-D-16-0048.1, 2018.

DeCarlo, P. F., Kimmel, J. R., Trimborn, A., Northway, M. J., Jayne, J. T., Aiken, A. C., Gonin, M., Fuhrer, K., Horvath, T., Docherty, K. S., Worsnop, D. R. and Jimenez, J. L.: Field-Deployable, High-Resolution, Time-of-Flight Aerosol Mass Spectrometer, Anal. Chem., 78(24), 8281–8289, doi:10.1021/ac061249n, 2006.

Ehn, M., Thornton, J. A., Kleist, E., Sipila, M., Junninen, H., Pullinen, I., Springer, M., Rubach, F., Tillmann, R., Lee, B., Lopez-Hilfiker, F., Andres, S., Acir, I.-H., Rissanen, M., Jokinen, T., Schobesberger, S., Kangasluoma, J., Kontkanen, J., Nieminen, T., Kurten, T., Nielsen, L. B., Jorgensen, S., Kjaergaard, H. G., Canagaratna, M., Dal Maso, M., Berndt, T., Petaja, T., Wahner, A., Kerminen, V.-M., Kulmala, M., Worsnop, D. R., Wildt, J. J., Mentel, T. F., Maso, M. D., Berndt, T., Petaja, T., Wahner, A., Kerminen, V.-M., Kulmala, M., Worsnop, D. R., Wildt, J. J. and Mentel, T. F.: A large source of low-volatility secondary organic aerosol, Nature, 506(7489), 476–479, doi:10.1038/nature13032, 2014.

Fisher, J. A., Jacob, D. J., Travis, K. R., Kim, P. S., Marais, E. A., Chan Miller, C., Yu, K., Zhu, L., Yantosca, R. M., Sulprizio, M. P., Mao, J., Wennberg, P. O., Crounse, J. D., Teng, A. P., Nguyen, T. B., St. Clair, J. M., Cohen, R. C., Romer, P., Nault, B. A., Wooldridge, P. J., Jimenez, J. L., Campuzano-Jost, P., Day, D. A., Hu, W., Shepson, P. B., Xiong, F., Blake, D. R., Goldstein, A. H., Misztal, P. K., Hanisco, T. F., Wolfe, G. M., Ryerson, T. B., Wisthaler, A. and Mikoviny, T.: Organic nitrate chemistry and its implications for nitrogen budgets in an isoprene- and

monoterpene-rich atmosphere: constraints from aircraft (SEAC^{4}RS) and ground-based (SOAS) observations in the Southeast US, Atmos. Chem. Phys., 16(9), 5969–5991, doi:10.5194/acp-16-5969-2016, 2016.

Gelaro, R., McCarty, W., Suárez, M. J., Todling, R., Molod, A., Takacs, L., Randles, C. A., Darmenov, A., Bosilovich, M. G., Reichle, R. and others: The modern-era retrospective analysis for research and applications, version 2 (MERRA-2), J. Clim., 30(14), 5419–5454, 2017.

Guenther, A. B., Jiang, X., Heald, C. L., Sakulyanontvittaya, T., Duhl, T., Emmons, L. K. and Wang, X.: The model of emissions of gases and aerosols from nature version 2.1 (MEGAN2.1): An extended and updated framework for modeling biogenic emissions, Geosci. Model Dev., 5(6), 1471–1492, doi:10.5194/gmd-5-1471-2012, 2012.

Hallquist, M., Wenger, J. C., Baltensperger, U., Rudich, Y., Simpson, D., Claeys, M., Dommen, J., Donahue, N. M., George, C., Goldstein, A. H., Hamilton, J. F., Herrmann, H., Hoffmann, T., Iinuma, Y., Jang, M., Jenkin, M. E., Jimenez, J. L., Kiendler-Scharr, A., Maenhaut, W., McFiggans, G., Mentel, T. F., Monod, A., Prévôt, A. S. H., Seinfeld, J. H., Surratt, J. D., Szmigielski, R. and Wildt, J.: The formation, properties and impact of secondary organic aerosol: current and emerging issues, Atmos. Chem. Phys., 9(14), 5155–5236, doi:10.5194/acp-9-5155-2009, 2009.

Iyer, S., Rissanen, M. P., Valiev, R., Barua, S., Krechmer, J. E., Thornton, J., Ehn, M. and Kurtén, T.: Molecular mechanism for rapid autoxidation in α-pinene ozonolysis, Nat. Commun., 12(1), 878, doi:10.1038/s41467-021-21172-w, 2021.

Jayne, J. T., Leard, D. C., Zhang, X., Davidovits, P., Smith, K. A., Kolb, C. E. and Worsnop, D. R.: Development of an Aerosol Mass Spectrometer for Size and Composition Analysis of Submicron Particles, Aerosol Sci. Technol., 33(1–2), 49–70, doi:10.1080/027868200410840, 2000.

Jimenez, J. L., Canagaratna, M. R., Donahue, N. M., Prevot, A. S. H., Zhang, Q., Kroll, J. H., DeCarlo, P. F., Allan, J. D., Coe, H., Ng, N. L., Aiken, A. C., Docherty, K. S., Ulbrich, I. M., Grieshop, A. P., Robinson, A. L., Duplissy, J., Smith, J. D., Wilson, K. R., Lanz, V. A., Hueglin, C., Sun, Y. L., Tian, J., Laaksonen, A., Raatikainen, T., Rautiainen, J., Vaattovaara, P., Ehn, M., Kulmala, M., Tomlinson, J. M., Collins, D. R., Cubison, M. J., Dunlea, J., Huffman, J. A., Onasch, T. B., Alfarra, M. R., Williams, P. I., Bower, K., Kondo, Y., Schneider, J., Drewnick, F., Borrmann, S., Weimer, S., Demerjian, K., Salcedo, D., Cottrell, L., Griffin, R., Takami, A., Miyoshi, T., Hatakeyama, S., Shimono, A., Sun, J. Y., Zhang, Y. M., Dzepina, K., Kimmel, J. R., Sueper, D., Jayne, J. T., Herndon, S. C., Trimborn, A. M., Williams, L. R., Wood, E. C., Middlebrook, A. M., Kolb, C. E., Baltensperger, U. and Worsnop, D. R.: Evolution of Organic Aerosols in the Atmosphere, Science (80-.)., 326(5959), 1525–1529, doi:10.1126/science.1180353, 2009.

Jokinen, T., Berndt, T., Makkonen, R., Kerminen, V.-M., Junninen, H., Paasonen, P., Stratmann, F., Herrmann, H., Guenther, A. B., Worsnop, D. R., Kulmala, M., Ehn, M. and Sipilä, M.: Production of extremely low volatile organic compounds from biogenic emissions: Measured yields and atmospheric implications., Proc. Natl. Acad. Sci. U. S. A., 112(23), 7123–8, doi:10.1073/pnas.1423977112, 2015.

Keller, C. A., Long, M. S., Yantosca, R. M., Da Silva, A. M., Pawson, S. and Jacob, D. J.: HEMCO v1.0: a versatile, ESMF-compliant component for calculating emissions in atmospheric models, Geosci. Model Dev., 7(4), 1409–1417, doi:10.5194/gmd-7-1409-2014, 2014.

Krapf, M., El Haddad, I., Bruns, E. A., Molteni, U., Daellenbach, K. R., Prévôt, A. S. H.,

Baltensperger, U., Dommen, J., Berndt, T., Richters, S., Kaethner, R., Voigtländer, J., Stratmann, F., Sipilä, M., Kulmala, M., Herrmann, H., Crounse, J. D., Nielsen, L. B., Jørgensen, S., Kjaergaard, H. G., Wennberg, P. O., Ehn, M., Thornton, J. A., Kleist, E., Sipila, M., Junninen, H., Pullinen, I., Springer, M., Rubach, F., Tillmann, R., Lee, B., et Al., Jokinen, T., Berndt, T., Makkonen, R., Kerminen, V.-M., Junninen, H., Paasonen, P., Stratmann, F., Herrmann, H., Guenther, A. B., Worsnop, D. R., et Al., Jokinen, T., Sipilä, M., Richters, S., Kerminen, V.-M., Paasonen, P., Stratmann, F., Worsnop, D., Kulmala, M., Ehn, M., Herrmann, H., Berndt, T., Mentel, T. F., Springer, M., Ehn, M., Kleist, E., Pullinen, I., Kurtén, T., Rissanen, M., Wahner, A., Wildt, J., Richters, S., Herrmann, H., Berndt, T., Rissanen, M. P., Kurtén, T., Sipilä, M., Thornton, J. A., Kangasluoma, J., Sarnela, N., Junninen, H., Jørgensen, S., Schallhart, S., Kajos, M. K., et Al., Heaton, K. J., Dreyfus, M. A., Wang, S., Johnston, M. V, Reinnig, M.-C., Warnke, J., Hoffmann, T., Ziemann, P. J., Aimanant, S., Ziemann, P. J., Docherty, K. S., Wu, W., Lim, Y. B., Ziemann, P. J., Mertes, P., Pfaffenberger, L., Dommen, J., Kalberer, M., Baltensperger, U., Nguyen, T. B., Bateman, A. P., Bones, D. L., et al.: Labile Peroxides in Secondary Organic Aerosol, Chem, 1(4), 603–616, doi:10.1016/j.chempr.2016.09.007, 2016.

Kulmala, M., Petäjä, T., Ehn, M., Thornton, J., Sipilä, M., Worsnop, D. R. and Kerminen, V.-M.: Chemistry of Atmospheric Nucleation: On the Recent Advances on Precursor Characterization and Atmospheric Cluster Composition in Connection with Atmospheric New Particle Formation, Annu. Rev. Phys. Chem., 65(1), doi:doi:10.1146/annurev-physchem-040412-110014, 2014.

Kurten, T., Rissanen, M. P., Mackeprang, K., Thornton, J. A., Hyttinen, N., Jorgensen, S., Ehn, M., Kjaergaard, H. G., Kurtén, T., Rissanen, M. P., Mackeprang, K., Thornton, J. A., Hyttinen, N., Jørgensen, S., Ehn, M. and Kjaergaard, H. G.: Computational Study of Hydrogen Shifts and Ring-Opening Mechanisms in α-Pinene Ozonolysis Products, J. Phys. Chem. A, 119(46), 11366–11375, doi:10.1021/acs.jpca.5b08948, 2015.

Lee, B. H., Mohr, C., Lopez-Hilfiker, F. D., Lutz, A., Hallquist, M., Lee, L., Romer, P., Cohen, R. C., Iyer, S., Kurten, T., Hu, W., Day, D. A., Campuzano-Jost, P., Jimenez, J. L., Xu, L., Ng, N. L., Guo, H., Weber, R. J., Wild, R. J., Brown, S. S., Koss, A., de Gouw, J., Olson, K., Goldstein, A. H., Seco, R., Kim, S., McAvey, K., Shepson, P. B., Starn, T., Baumann, K., Edgerton, E. S., Liu, J., Shilling, J. E., Miller, D. O., Brune, W., Schobesberger, S., D'Ambro, E. L., Thornton, J. A., Kurtén, T., Hu, W., Day, D. A., Campuzano-Jost, P., Jimenez, J. L., Xu, L., Ng, N. L., Guo, H., Weber, R. J., Wild, R. J., Brown, S. S., Koss, A., de Gouw, J., Olson, K., Goldstein, A. H., Seco, R., Kim, S., McAvey, K., Shepson, P. B., Starn, T., Baumann, K., Edgerton, E. S., Liu, J., Shilling, J. E., Miller, D. O., Brune, W., Schobesberger, S., D\textquoterightAmbro, E. L. and Thornton, J. A.: Highly functionalized organic nitrates in the southeast United States: Contribution to secondary organic aerosol and reactive nitrogen budgets, Proc. Natl. Acad. Sci., 113(6), 1516–1521, doi:10.1073/pnas.1508108113, 2016.

Lee, B. H., Lopez-Hilfiker, F. D., D'Ambro, E. L., Zhou, P., Boy, M., Petaja, T., Hao, L., Virtanen, A. and Thornton, J. A.: Semi-volatile and highly oxygenated gaseous and particulate organic compounds observed above a boreal forest canopy, Atmos. Chem. Phys., 18(15), 11547–11562, doi:10.5194/acp-18-11547-2018, 2018.

Lee, B. H., D'Ambro, E. L., Lopez-Hilfiker, F. D., Schobesberger, S., Mohr, C., Zawadowicz, M. A., Liu, J., Shilling, J. E., Hu, W., Palm, B. B., Jimenez, J. L., Hao, L., Virtanen, A., Zhang, H., Goldstein, A. H., Pye, H. O. T. and Thornton, J. A.: Resolving Ambient Organic Aerosol Formation and

887 Aging Pathways with Simultaneous Molecular Composition and Volatility Observations, ACS
888 Earth Sp. Chem., 4(3), 391–402, doi:10.1021/acsearthspacechem.9b00302, 2020.
889Liu, H., Jacob, D. J., Bey, I. and Yantosca, R. M.: Constraints from 210Pb and 7Be on wet
890 deposition and transport in a global three-dimensional chemical tracer model driven by
891 assimilated meteorological fields, J. Geophys. Res. Atmos., 106(D11), 12109–12128,
892 doi:https://doi.org/10.1029/2000JD900839, 2001.
893Lopez-Hilfiker, F. D., Mohr, C., Ehn, M., Rubach, F., Kleist, E., Wildt, J., Mentel, T. F., Lutz, A.,
894 Hallquist, M., Worsnop, D. and Thornton, J. A.: A novel method for online analysis of gas and
895 particle composition: description and evaluation of a Filter Inlet for Gases and AEROsols
896 (FIGAERO), , 7(4), 983–1001, doi:10.5194/amt-7-983-2014, 2014.
897Lopez-Hilfiker, F. D., Mohr, C., D'Ambro, E. L., Lutz, A., Riedel, T. P., Gaston, C. J., Iyer, S., Zhang, Z.,
898 Gold, A., Surratt, J. D., Lee, B. H., Kurten, T., Hu, W. W., Jimenez, J., Hallquist, M. and Thornton,
899 J. A.: Molecular Composition and Volatility of Organic Aerosol in the Southeastern U.S.:
900 Implications for IEPOX Derived SOA, Environ. Sci. Technol., 50(5), 2200–2209,
901 doi:10.1021/acs.est.5b04769, 2016.
902Mao, J., Jacob, D. J., Evans, M. J., Olson, J. R., Ren, X., Brune, W. H., St. Clair, J. M., Crounse, J. D.,
903 Spencer, K. M., Beaver, M. R., Wennberg, P. O., Cubison, M. J., Jimenez, J. L., Fried, A.,
904 Weibring, P., Walega, J. G., Hall, S. R., Weinheimer, A. J., Cohen, R. C., Chen, G., Crawford, J.
905 H., McNaughton, C., Clarke, A. D., Jaeglé, L., Fisher, J. A., Yantosca, R. M., Le Sager, P. and
906 Carouge, C.: Chemistry of hydrogen oxide radicals (HOx) in the Arctic troposphere in spring,
907 Atmos. Chem. Phys., 10(13), 5823–5838, doi:10.5194/acp-10-5823-2010, 2010.
908Mao, J., Paulot, F., Jacob, D. J., Cohen, R. C., Crounse, J. D., Wennberg, P. O., Keller, C. A., Hudman,
909 R. C., Barkley, M. P. and Horowitz, L. W.: Ozone and organic nitrates over the eastern United
910 States: Sensitivity to isoprene chemistry, J. Geophys. Res. Atmos., 118(19), 11256–11268,
911 doi:10.1002/jgrd.50817, 2013.
912Martin, S. T., Artaxo, P., Machado, L. A. T., Manzi, A. O., Souza, R. A. F., Schumacher, C., Wang, J.,
913 Andreae, M. O., Barbosa, H. M. J., Fan, J., Fisch, G., Goldstein, A. H., Guenther, A., Jimenez, J.
914 L., Pöschl, U., Silva Dias, M. A., Smith, J. N. and Wendisch, M.: Introduction: Observations and
915 Modeling of the Green Ocean Amazon (GoAmazon2014/5), Atmos. Chem. Phys., 16(8),
916 4785–4797, doi:10.5194/acp-16-4785-2016, 2016.
917Massoli, P., Stark, H., Canagaratna, M. R., Krechmer, J. E., Xu, L., Ng, N. L., Mauldin, R. L., Yan, C.,
918 Kimmel, J., Misztal, P. K., Jimenez, J. L., Jayne, J. T. and Worsnop, D. R.: Ambient
919 Measurements of Highly Oxidized Gas-Phase Molecules during the Southern Oxidant and
920 Aerosol Study (SOAS) 2013, ACS Earth Sp. Chem., 2(7), 653–672,
921 doi:10.1021/acsearthspacechem.8b00028, 2018.
922McDonald, B. C., de Gouw, J. A., Gilman, J. B., Jathar, S. H., Akherati, A., Cappa, C. D., Jimenez, J.
923 L., Lee-Taylor, J., Hayes, P. L., McKeen, S. A., Cui, Y. Y., Kim, S.-W., Gentner, D. R.,
924 Isaacman-VanWertz, G., Goldstein, A. H., Harley, R. A., Frost, G. J., Roberts, J. M., Ryerson, T.
925 B. and Trainer, M.: Volatile chemical products emerging as largest petrochemical source of
926 urban organic emissions, Science (80-.)., 359(6377), 760–764, doi:10.1126/science.aaq0524,
927 2018.
928McFiggans, G., Mentel, T. F., Wildt, J., Pullinen, I., Kang, S., Kleist, E., Schmitt, S., Springer, M.,
929 Tillmann, R., Wu, C., Zhao, D., Hallquist, M., Faxon, C., Le Breton, M., Hallquist, A. M.,
930 Simpson, D., Bergstroem, R., Jenkin, M. E., Ehn, M., Thornton, J. A., Alfarra, M. R., Bannan, T.

J., Percival, C. J., Priestley, M., Topping, D. and Kiendler-Scharr, A.: Secondary organic aerosol reduced by mixture of atmospheric vapours, Nature, 565(7741), 587–593, doi:10.1038/s41586-018-0871-y, 2019.

Mentel, T. F., Springer, M., Ehn, M., Kleist, E., Pullinen, I., Kurtén, T., Rissanen, M., Wahner, A. and Wildt, J.: Formation of highly oxidized multifunctional compounds: autoxidation of peroxy radicals formed in the ozonolysis of alkenes – deduced from structure–product relationships, Atmos. Chem. Phys., 15(12), 6745–6765, doi:10.5194/acp-15-6745-2015, 2015.

Messina, P., Lathière, J., Sindelarova, K., Vuichard, N., Granier, C., Ghattas, J., Cozic, A. and Hauglustaine, D. A.: Global biogenic volatile organic compound emissions in the ORCHIDEE and MEGAN models and sensitivity to key parameters, Atmos. Chem. Phys., 16(22), 14169–14202, doi:10.5194/acp-16-14169-2016, 2016.

Orlando, J. J., Tyndall, G. S. and Wallington, T. J.: The Atmospheric Chemistry of Alkoxy Radicals, Chem. Rev., 103(12), 4657–4690, doi:10.1021/cr020527p, 2003.

Öström, E., Putian, Z., Schurgers, G., Mishurov, M., Kivekäs, N., Lihavainen, H., Ehn, M., Rissanen, M. P., Kurtén, T., Boy, M., Swietlicki, E. and Roldin, P.: Modeling the role of highly oxidized multifunctional organic molecules for the growth of new particles over the boreal forest region, Atmos. Chem. Phys., 17(14), 8887–8901, doi:10.5194/acp-17-8887-2017, 2017.

Palen, E. J., Allen, D. T., Pandis, S. N., Paulson, S. E., Seinfeld, J. H. and Flagan, R. C.: Fourier transform infrared analysis of aerosol formed in the photo-oxidation of isoprene and β-pinene, Atmos. Environ. Part A. Gen. Top., 26(7), 1239–1251, doi:https://doi.org/10.1016/0960-1686(92)90385-X, 1992.

Pandis, S. N., Harley, R. A., Cass, G. R. and Seinfeld, J. H.: Secondary organic aerosol formation and transport, Atmos. Environ. Part A. Gen. Top., 26(13), 2269–2282, doi:https://doi.org/10.1016/0960-1686(92)90358-R, 1992.

Petaja, T., O'Connor, E. J., Moisseev, D., Sinclair, V. A. V. A., Manninen, A. J. A. J., Vaananen, R., von Lerber, A., Thorntoton, J. A., Nicocoll, K., Petersen, W., Chandrasekar, V., Smith, J. N., Winkler, P. M., Krueger, O., Hakola, H., Timonen, H., Brus, D., Laurila, T., Asmi, E., Riekkola, M.-L., Mona, L., Massoli, P., Engelmann, R., Kompppula, M., Wang, J., Kuang, C., Baeck, J., Virtanen, A., Levula, J., Ritsche, M., Hickmon, N., Petäjä, T., O'Connor, E. J., Moisseev, D., Sinclair, V. A. V. A., Manninen, A. J. A. J., Väänänen, R., von Lerber, A., Thornton, J. A., Nicoll, K., Petersen, W., Chandrasekar, V., Smith, J. N., Winkler, P. M., Krüger, O., Hakola, H., Timonen, H., Brus, D., Laurila, T., Asmi, E., Riekkola, M.-L., Mona, L., Massoli, P., Engelmann, R., Komppula, M., Wang, J., Kuang, C., Bäck, J., Virtanen, A., Levula, J., Ritsche, M. and Hickmon, N.: BAECC: A Field Campaign to Elucidate the Impact of Biogenic Aerosols on Clouds and Climate, Bull. Am. Meteorol. Soc., 97(10), 1909–1928, doi:10.1175/BAMS-D-14-00199.1, 2016.

Pospisilova, V., Lopez-Hilfiker, F. D., Bell, D. M., El Haddad, I., Mohr, C., Huang, W., Heikkinen, L., Xiao, M., Dommen, J., Prevot, A. S. H., Baltensperger, U. and Slowik, J. G.: On the fate of oxygenated organic molecules in atmospheric aerosol particles, Sci. Adv., 6(11), doi:10.1126/sciadv.aax8922, 2020.

Pullinen, I., Schmitt, S., Kang, S., Sarrafzadeh, M., Schlag, P., Andres, S., Kleist, E., Mentel, T. F., Rohrer, F., Springer, M., Tillmann, R., Wildt, J., Wu, C., Zhao, D., Wahner, A., and Kiendler-Scharr, A.: Impact of NOx on secondary organic aerosol (SOA) formation from α-pinene and β-pinene photooxidation: the role of highly oxygenated organic nitrates, Atmos. Chem. Phys., 20, 10125–10147, https://doi.org/10.5194/acp-20-10125-2020, 2020

975Richters, S., Herrmann, H. and Berndt, T.: Highly Oxidized RO2 Radicals and Consecutive Products
976 from the Ozonolysis of Three Sesquiterpenes, Environ. Sci. \& Technol., 50(5), 2354–2362,
977 doi:10.1021/acs.est.5b05321, 2016.
978Roldin, P., Ehn, M., Kurtén, T., Olenius, T., Rissanen, M. P., Sarnela, N., Elm, J., Rantala, P., Hao, L.,
979 Hyttinen, N., Heikkinen, L., Worsnop, D. R., Pichelstorfer, L., Xavier, C., Clusius, P., Öström, E.,
980 Petäjä, T., Kulmala, M., Vehkamäki, H., Virtanen, A., Riipinen, I. and Boy, M.: The role of
981 highly oxygenated organic molecules in the Boreal aerosol-cloud-climate system, Nat.
982 Commun., 10(1), 4370, doi:10.1038/s41467-019-12338-8, 2019.
983de Sa, S. S., Palm, B. B., Campuzano-Jost, P., Day, D. A., Hu, W., Isaacman-VanWertz, G., Yee, L. D.,
984 Brito, J., Carbone, S., Ribeiro, I. O., Cirino, G. G., Liu, Y., Thalman, R., Sedlacek, A., Funk, A.,
985 Schumacher, C., Shilling, J. E., Schneider, J., Artaxo, P., Goldstein, A. H., Souza, R. A. F., Wang,
986 J., McKinney, K. A., Barbosa, H., Alexander, M. L., Jimenez, J. L. and Martin, S. T.: Urban
987 influence on the concentration and composition of submicron particulate matter in central
988 Amazonia, Atmos. Chem. Phys., 18(16), 12185–12206, doi:10.5194/acp-18-12185-2018,
989 2018.
990Travis, K. R., Jacob, D. J., Fisher, J. A., Kim, P. S., Marais, E. A., Zhu, L., Yu, K., Miller, C. C., Yantosca,
991 R. M., Sulprizio, M. P., Thompson, A. M., Wennberg, P. O., Crounse, J. D., St Clair, J. M., Cohen,
992 R. C., Laughner, J. L., Dibb, J. E., Hall, S. R., Ullmann, K., Wolfe, G. M., Pollack, I. B., Peischl, J.,
993 Neuman, J. A. and Zhou, X.: Why do models overestimate surface ozone in the Southeast
994 United States?, Atmos. Chem. Phys., 16(21), 13561–13577, doi:10.5194/acp-16-13561-2016,
995 2016.
996Wang, J., Krejci, R., Giangrandel, S., Kuang, C., Barbosa, H. M. J., Brito, J., Carbone, S., Chi, X.,
997 Comstock, J., Ditas, F., Lavric, J., Manninen, H. E., Mei, F., Moran-Zuloaga, D., Poehlker, C.,
998 Poehlker, M. L., Saturno, J., Schmid, B., Souza, R. A. F., Springston, S. R., Tomlinson, J. M., Toto,
999 T., Walter, D., Wimmer, D., Smith, J. N., Kulmala, M., Machado, L. A. T., Artaxo, P., Andreae, M.
1000 O., Petaja, T. and Martin, S. T.: Amazon boundary layer aerosol concentration sustained by
1001 vertical transport during rainfall, Nature, 539(7629), 416–419, doi:10.1038/nature19819,
1002 2016.
1003Weber, J., Archer-Nicholls, S., Griffiths, P., Berndt, T., Jenkin, M., Gordon, H., Knote, C. and
1004 Archibald, A. T.: CRI-HOM: A novel chemical mechanism for simulating highly oxygenated
1005 organic molecules (HOMs) in global chemistry--aerosol--climate models, Atmos. Chem. Phys.,
1006 20(18), 10889–10910, doi:10.5194/acp-20-10889-2020, 2020.
1007Wesely, M. L.: Parameterization of surface resistances to gaseous dry deposition in regional-scale
1008 numerical models, Atmos. Environ., 23(6), 1293–1304,
1009 doi:https://doi.org/10.1016/0004-6981(89)90153-4, 1989.
1010Xu, L., Pye, H. O. T., He, J., Chen, Y., Murphy, B. N. and Ng, N. L.: Experimental and model
1011 estimates of the contributions from biogenic monoterpenes and sesquiterpenes to
1012 secondary organic aerosol in the southeastern United States, Atmos. Chem. Phys., 18(17),
1013 12613–12637, doi:10.5194/acp-18-12613-2018, 2018.
1014Xu, L., Møller, K. H., Crounse, J. D., Otkjær, R. V., Kjaergaard, H. G. and Wennberg, P. O.:
1015 Unimolecular reactions of peroxy radicals formed in the oxidation of α-Pinene and β-Pinene
1016 by hydroxyl radicals, J. Phys. Chem. A, doi:10.1021/acs.jpca.8b11726, 2019.
1017Zawadowicz, M. A., Lee, B. H., Shrivastava, M., Zelenyuk, A., Zaveri, R. A., Flynn, C., Thornton, J. A.
1018 and Shilling, J. E.: Photolysis Controls Atmospheric Budgets of Biogenic Secondary Organic

Aerosol, Environ. Sci. \& Technol., 54(7), 3861–3870, doi:10.1021/acs.est.9b07051, 2020.

Zhang, H., Yee, L. D., Lee, B. H., Curtis, M. P., Worton, D. R., Isaacman-VanWertz, G., Offenberg, J. H., Lewandowski, M., Kleindienst, T. E., Beaver, M. R., Holder, A. L., Lonneman, W. A., Docherty, K. S., Jaoui, M., Pye, H. O. T., Hu, W., Day, D. A., Campuzano-Jost, P., Jimenez, J. L., Guo, H., Weber, R. J., de Gouw, J., Koss, A. R., Edgerton, E. S., Brune, W., Mohr, C., Lopez-Hilfiker, F. D., Lutz, A., Kreisberg, N. M., Spielman, S. R., Hering, S. V, Wilson, K. R., Thornton, J. A. and Goldstein, A. H.: Monoterpenes are the largest source of summertime organic aerosol in the southeastern United States, Proc. Natl. Acad. Sci. U. S. A., 115(9), 2038–2043, doi:10.1073/pnas.1717513115, 2018.

Zhang, L., Gong, S., Padro, J. and Barrie, L.: A size-segregated particle dry deposition scheme for an atmospheric aerosol module, Atmos. Environ., 35(3), 549–560, doi:https://doi.org/10.1016/S1352-2310(00)00326-5, 2001.

Zhang, S.-H., Shaw, M., Seinfeld, J. H. and Flagan, R. C.: Photochemical aerosol formation from α-pinene- and β-pinene, J. Geophys. Res. Atmos., 97(D18), 20717–20729, doi:https://doi.org/10.1029/92JD02156, 1992.

Zhao, B., Shrivastava, M., Donahue, N. M., Gordon, H., Schervish, M., Shilling, J. E., Zaveri, R. A., Wang, J., Andreae, M. O., Zhao, C., Gaudet, B., Liu, Y., Fan, J. and Fast, J. D.: High concentration of ultrafine particles in the Amazon free troposphere produced by organic new particle formation, Proc. Natl. Acad. Sci., 117(41), 25344–25351, doi:10.1073/pnas.2006716117, 2020.

Zhao, Y., Thornton, J. A. and Pye, H. O. T.: Quantitative constraints on autoxidation and dimer formation from direct probing of monoterpene-derived peroxy radical chemistry, Proc. Natl. Acad. Sci. U. S. A., 115(48), 12142–12147, doi:10.1073/pnas.1812147115, 2018.

Zhu, J., Penner, J.E., Yu, F., Sillman, S., Andreae, M. O., Coe, H. Decrease in radiative forcing by organic aerosol nucleation, climate, and land use change, Nat. Commun., **10,** 423 (2019). https://doi.org/10.1038/s41467-019-08407-7